# Chromatin-remodeling SWI/SNF complex regulates coenzyme Q$_6$ synthesis and a metabolic shift to respiration in yeast

**Agape M. Awad**[‡§1], **Srivats Venkataramanan**[§¶1], **Anish Nag**[‡§], **Anoop Raj Galivanche**[¶], **Michelle C. Bradley**[‡§], **Lauren T. Neves**[§¶], **Stephen Douglass**[¶], **Catherine F. Clarke**[‡§2], and **Tracy L. Johnson**[§¶3]

*From the ‡Department of Chemistry and Biochemistry, the §Molecular Biology Institute, and the ¶Department of Molecular Cell and Developmental Biology, UCLA, Los Angeles, California 90095*

Edited by Dennis R. Voelker

**Despite its relatively streamlined genome, there are many important examples of regulated RNA splicing in *Saccharomyces cerevisiae*. Here, we report a role for the chromatin remodeler SWI/SNF in respiration, partially via the regulation of splicing. We find that a nutrient-dependent decrease in Snf2 leads to an increase in splicing of the *PTC7* transcript. The spliced *PTC7* transcript encodes a mitochondrial phosphatase regulator of biosynthesis of coenzyme Q$_6$ (ubiquinone or CoQ$_6$) and a mitochondrial redox-active lipid essential for electron and proton transport in respiration. Increased splicing of *PTC7* increases CoQ$_6$ levels. The increase in *PTC7* splicing occurs at least in part due to down-regulation of ribosomal protein gene expression, leading to the redistribution of spliceosomes from this abundant class of intron-containing RNAs to otherwise poorly spliced transcripts. In contrast, a protein encoded by the non-spliced isoform of *PTC7* represses CoQ$_6$ biosynthesis. Taken together, these findings uncover a link between Snf2 expression and the splicing of *PTC7* and establish a previously unknown role for the SWI/SNF complex in the transition of yeast cells from fermentative to respiratory modes of metabolism.**

Similar to other eukaryotic genomes, genes in *Saccharomyces cerevisiae* may be interrupted by non-coding sequences, called introns. Introns are removed from the pre-mRNA through the action of the spliceosome, a macromolecular machine composed of five small nuclear ribonucleoproteins. The spliceosome recognizes consensus sequence signals on the pre-mRNA, termed splice sites, by which it subsequently binds to the intron and catalyzes its removal via two transesterification reactions (1). Pre-mRNA splicing is critical for accurate gene expression in all eukaryotes, and there is significant evidence that alterations in microenvironments, such as changes in the chromatin state or chromatin-modifying factors, can affect splicing outcomes (1). However, the mechanisms for how chromatin and chromatin factors influence splicing are not completely understood.

Although the genome of *S. cerevisiae* contains a smaller number of introns than metazoan genomes, there are, nonetheless, numerous examples of intron-dependent gene regulation (2). The largest functional class of intron-containing genes (ICGs)[4] in budding yeast is ribosomal protein genes (RPGs) that encode the protein components of the ribosome. Therefore, the energy-intensive process of translation is under the heavy regulatory control of the spliceosome, such that splicing of RPGs can be finely tuned to the cells' environmental conditions and to nutrient availability (3).

Interestingly, this enrichment of introns within RPGs impacts the splicing of, as well as provides an opportunity for the regulation of, other ICGs within the yeast genome. About a third of yeast introns occur in RPGs, and the high transcription levels of these genes means that about 90% of the intron load encountered by the spliceosome is from this one functional class of genes (4). Indeed, the prevalence of RPG introns functions to titrate spliceosomes away from other introns, especially those containing suboptimal splice sites. Conversely, down-regulating RPG expression promotes the splicing of transcripts harboring suboptimal splice sites. This effect is perhaps best described during the process of yeast meiosis. Under conditions of vegetative growth, a number of meiosis-specific ICGs are expressed, but they possess suboptimal splice sites and are therefore poorly recognized by the spliceosome and suboptimally spliced. However, upon the down-regulation of RPGs during meiosis, increased availability of the previously limiting pool of spliceosomes leads to improved splicing efficiency of introns in meiosis-specific transcripts (5, 6).

[4] The abbreviations used are: ICG, intron-containing gene; RPG, ribosomal protein gene; ns, non-spliced; s, spliced; CoQ, coenzyme Q; DMQ$_6$, 5-demethoxy-Q$_6$; 4HB, 4-hydroxybenzoic acid; HHB, 3-hexaprenyl-4-hydroxybenzoic acid; qPCR, quantitative PCR; TOR, target of rapamycin.

There are other important examples of intron-based regulation in *S. cerevisiae*, especially among ICGs with non-consensus splice sites (7, 8). One such gene is *PTC7*, which encodes a $Mg^{2+}/Mn^{2+}$-dependent, type 2C serine/threonine protein phosphatase (9). The intron within *PTC7* is particularly intriguing because it contains a non-consensus branch-point sequence, rendering its splicing relatively inefficient under logarithmic growth conditions. The *PTC7* intron lacks a premature termination codon and is translated in-frame. The longer, non-spliced (ns) form of the *PTC7* RNA encodes a longer protein (Ptc7$_{ns}$) that contains a single trans-membrane helix located near the N terminus but is otherwise identical to the protein isoform derived from the spliced *PTC7* RNA (Ptc7$_s$). The read-through nature of the *PTC7* intron is conserved across yeast species, indicating potential functionality for both Ptc7$_s$ and Ptc7$_{ns}$ protein isoforms (10). Ptc7$_{ns}$ has been localized to the nuclear membrane, whereas Ptc7$_s$ is located within mitochondria (10). Ptc7$_s$ has been implicated in regulation of coenzyme Q (also termed ubiquinone or CoQ) biosynthesis via its phosphatase activity (11, 12). However, mechanisms of regulation of Ptc7 itself and the role of the evolutionarily conserved Ptc7$_{ns}$ isoform remain outstanding questions.

CoQ is a redox-active lipid composed of a fully substituted benzoquinone ring and a polyisoprenoid tail and is required for mitochondrial electron transport. The length of the polyisoprenoid group is species-specific; humans produce CoQ$_{10}$, and *S. cerevisiae* produce CoQ$_6$, with 10 and 6 isoprene units, respectively. The primary role of CoQ in the inner mitochondrial membrane is to accept the electrons from complex I and complex II and pass those electrons to complex III. Several other metabolic pathways, such as pyrimidine synthesis, sulfide oxidation, and fatty acid $\beta$-oxidation, rely on CoQ as an electron carrier (13). CoQ is present in all intracellular membranes, where it may function as a lipid-soluble antioxidant. Several human syndromes, including encephalomyopathy, ataxia, cerebellar atrophy, myopathy, and steroid-resistant nephrotic syndrome, are linked to primary deficiencies in CoQ biosynthesis (14–17).

Mitochondrial proteins are responsible for facilitating the biosynthesis of CoQ$_6$ in *S. cerevisiae* and include Coq1–Coq11 (18). Many of the Coq proteins necessary for the biosynthesis of CoQ$_6$ associate in a high-molecular weight complex (termed the "CoQ-synthome"), a multisubunit complex that is peripherally associated with the inner mitochondrial membrane on the matrix side (18). Ptc7$_s$ has been shown to localize to the mitochondria, where it is thought to regulate the phosphorylation state of Coq7 (11) and/or influence mitochondrial respiratory metabolism (12). In the former case, Ptc7s is believed to control, at least in part, the phosphorylation state of the Coq7 polypeptide, which modulates its hydroxylase activity. Coq7 catalyzes the hydroxylation of 5-demethoxy-Q$_6$ (DMQ$_6$), the penultimate step in the biosynthesis of CoQ$_6$ in yeast (19, 20).

The conserved SWI/SNF complex utilizes ATP hydrolysis by Snf2, the catalytic subunit, to disrupt specific histone–DNA contacts, resulting in the sliding or eviction of nucleosomes from the locus. As a result, Snf2 activity contributes to transcriptional regulation (21, 22). The genome-wide distribution of SWI/SNF is responsive to conditions of stress, and the complex is required for transcription of a number of stress response genes (23, 24). We have previously reported that levels of Snf2 change in response to nutrient conditions. We have also reported that the change in Snf2 leads to changes in levels of RPG transcripts, thereby regulating splicing outcomes (6). Here, we show that changes in levels of Snf2 modulate the CoQ$_6$ biosynthetic pathway in *S. cerevisiae*. First, we show that deletion of Snf2 alters the relative levels of Ptc7$_s$ and Ptc7$_{ns}$ isoforms in yeast and increases both the rate of synthesis and steady-state levels of CoQ$_6$. This is due to down-regulation of RPG transcripts and an increase in the available pool of spliceosomes. Moreover, we find that the Snf2 protein is down-regulated over time under batch growth conditions and nutrient depletion, and together with a concomitant increase in the splicing of *PTC7*, this leads to higher CoQ$_6$ levels in preparation for the transition from a fermentative mode of metabolism to a respiratory mode. Furthermore, we show that the two Ptc7 isoforms have opposing effects on the CoQ$_6$ biosynthetic pathway, which may explain contradictory reports in the literature about the effects of Ptc7 on CoQ$_6$ levels (11, 12). Importantly, although Snf2 is down-regulated in response to nutrient-depleted conditions, it is nonetheless required for growth on nonfermentable carbon sources, suggesting that dynamic control of Snf2 levels is crucial for the transition from fermentation to respiration.

## Results

### Deletion of Snf2 leads to enhanced splicing of PTC7 and a shift in the ratios of Ptc7 protein isoforms

Previously published RNA sequencing data for yeast lacking Snf2, the core ATPase component of the SWI/SNF complex (GEO accession number GSE94404), revealed an increase in splicing of a number of introns (6). Satisfyingly, the greatest improvement in splicing upon deletion of Snf2 is experienced by *RPL22B*, via a previously described mechanism consistent with down-regulation of RPG expression (25). The next two largest improvements in splicing efficiency are experienced by *YBR062C* (an ORF of unknown function) and *PTC7*, a previously described type 2C serine-threonine mitochondrial phosphatase that contains all 11 canonical motifs of the PPM family (type 2C) protein phosphatases, previously reported to play a role in CoQ$_6$ biosynthesis in yeast (11) (Fig. 1*A*). This increase in splicing of *PTC7* RNA was verified by RT-PCR (Fig. 1*B*). In addition, the results from the RNA-seq and RT-PCR were also independently verified by qPCR (data not shown). It has previously been demonstrated that increased splicing of poorly recognized introns can be achieved by decreased expression of competing, highly expressed RPGs (5). Furthermore, we have shown that deletion of Snf2 causes *en masse* down-regulation of RPGs and consequent improvement in splicing of a large number of introns (6). RPG down-regulation in the absence of Snf2 was validated by RT-PCR analysis. For example, expression of RPS16A and RPL34B, two intron-containing RPGs, is down-regulated in *snf2Δ* yeast compared with WT (Fig. 1*C*).

The *PTC7* transcript makes two distinct protein isoforms, one from the nonspliced and one from the spliced RNA. The spliced isoform (Ptc7$_s$) localizes to the mitochondria, whereas
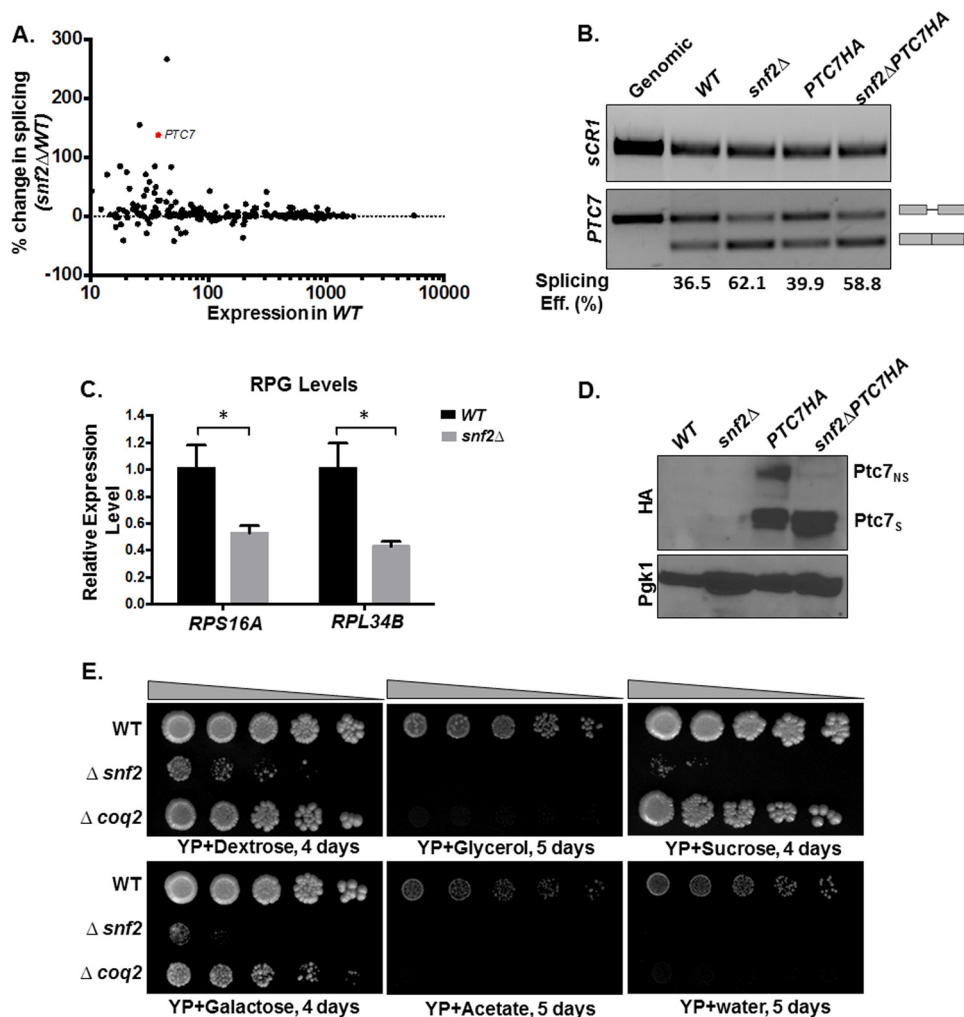
**Figure 1. Deletion of *SNF2* enhances splicing of *PTC7* and the steady-state levels of the short Ptc7 protein isoform.** *A*, deletion of *SNF2* enhances splicing of a subset of yeast RNAs, including *PTC7*. The scatter plot shows changes in splicing of individual introns in *snf2Δ* yeast over WT plotted against expression in WT. Percentage change in splicing is calculated as 100 × (S.E. in *snf2Δ* − S.E. in WT)/(S.E. in WT). *PTC7* is represented by the *red dot*. *B*, expression and splicing of *PTC7* in *WT* and *snf2Δ* yeast with HA-tagged and untagged Ptc7. Semiquantitative analysis of splicing efficiency of *PTC7* mRNA is indicated *below* each *lane*. sCR1 served as an internal control. *Gray bars*, exons of the RNA; *thin gray line*, intron. *C*, RT-qPCR measurement of selected intron-containing RPG transcripts between WT and *snf2Δ* yeast strains. Shown is the mean of three biological replicates (unpaired Student's *t* test; *, $p < 0.05$). *Error bars*, S.D. *D*, deletion of *SNF2* affects steady-state levels of HA-tagged Ptc7 proteins. Proteins derived from the nonspliced and spliced forms of the *PTC7*-HA RNA are denoted as *Ptc7$_{ns}$HA* and *Ptc7$_s$HA*, respectively. Pgk1 (phosphoglycerate kinase 1) served as a loading control. *E*, serial dilutions (5-fold) of WT BY4741, *snf2Δ*, and *coq2Δ* (negative respiratory-deficient control; W303 background, because the deletion is unstable in the BY background) on YP agar plates with the indicated carbon sources.

the nonspliced isoform (Ptc7$_{ns}$) has been reported to localize to the nuclear envelope (10). The *PTC7* gene was endogenously HA-tagged, and Western blot analysis demonstrated that deletion of Snf2 leads to an increase in the levels of Ptc7$_s$ compared with Ptc7$_{ns}$ (Fig. 1*D*). It is noteworthy that the increase in the ratio of Ptc7$_s$/Ptc7$_{ns}$ polypeptides in the WT and *snf2Δ* cells appears to be greater than the increased ratio of spliced/unspliced RNA.
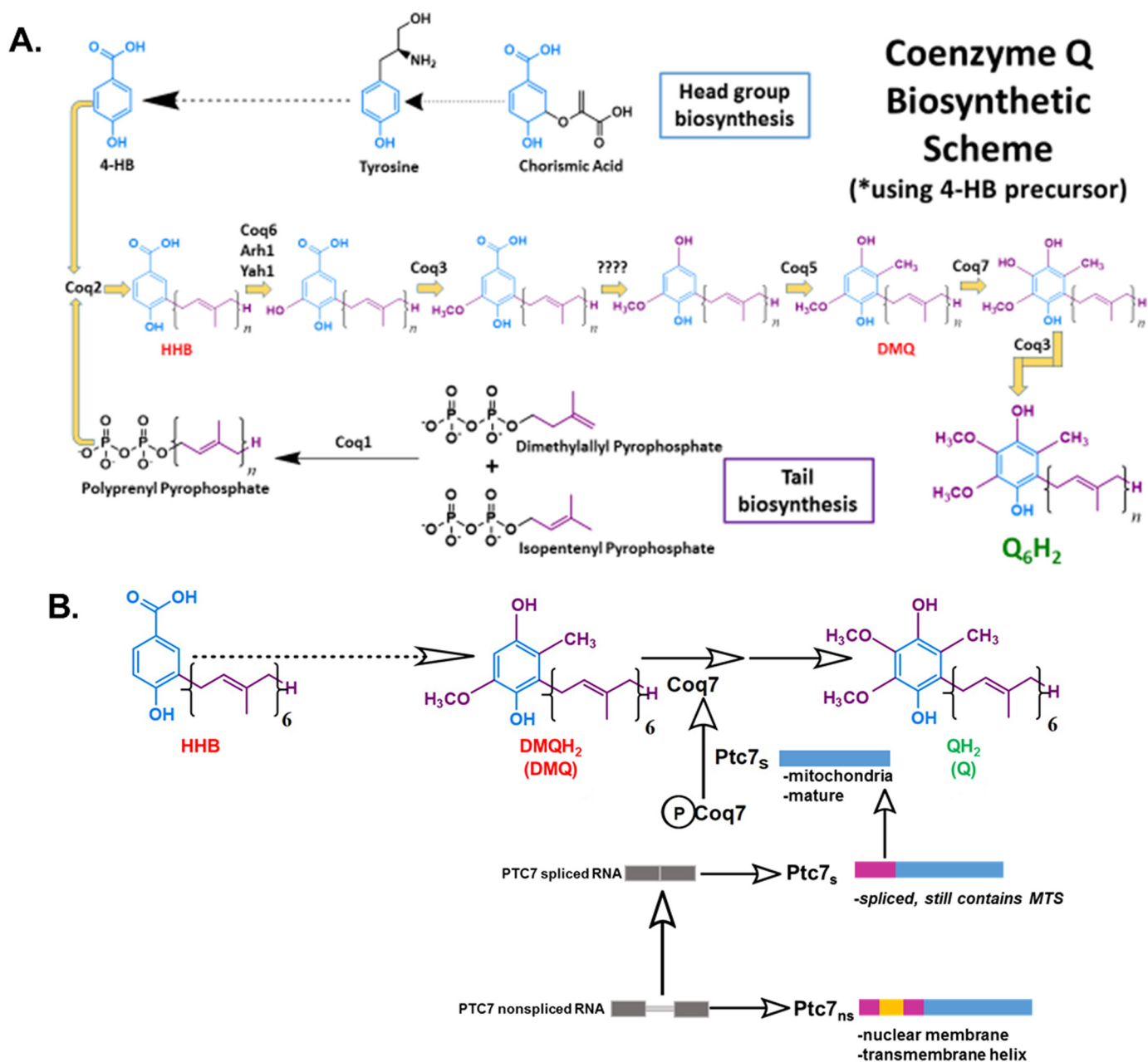
It has previously been demonstrated that yeast strains lacking Snf2 fail to grow on non-fermentable carbon sources, such as glycerol or acetate (26). However, *snf2Δ* mutants frequently incur secondary mutations, and the growth of such strains can resemble WT. Therefore, growth on fermentable and non-fermentable carbon sources was used as a quality control for the assessment of the *bona fide* phenotype (24) of *snf2Δ* prior to each experiment (Fig. 1*E*).

### Deletion of Snf2 leads to increased CoQ$_6$ synthesis in yeast and improves the flux from DMQ$_6$ to CoQ$_6$

Ptc7$_s$ has previously been described as playing a role in regulating CoQ$_6$ synthesis in *S. cerevisiae* (11). A schematic of the entire CoQ$_6$ biosynthetic pathway with 4-hydroxybenzoic acid as the ring precursor and the role of Ptc7 is detailed in Fig. 2*A*. Ptc7$_s$ is thought to enhance CoQ$_6$ biosynthesis via its activation of Coq7 and subsequent catalysis of the hydroxylation of DMQ$_6$, the penultimate step of CoQ$_6$ biosynthesis (Fig. 2*B*) (11, 27).

$^{13}$C$_6$-Labeled 4-hydroxybenzoic acid ($^{13}$C$_6$-4HB), a ring precursor for Q biosynthesis, was used to determine the levels of $^{13}$C$_6$-CoQ$_6$ biosynthesis in WT *versus* *snf2Δ* yeast grown to similar culture densities. The absence of Snf2 causes increased steady-state levels of CoQ$_6$ and increased *de novo* biogenesis of $^{13}$C$_6$-CoQ$_6$ (Fig. 3*A*). Additionally, there are significant changes in the levels of *de novo* synthesized DMQ$_6$, as well as 3-hexa-

**Figure 2. CoQ₆ biosynthetic pathway in *S. cerevisiae* and role of Ptc7ₛ isoform on Coq7 phosphorylation and function.** *A*, schematic of CoQ₆ biosynthetic pathway in yeast using 4HB as a ring precursor, ultimately forming the reduced CoQ₆H₂ product *in vivo*. The *question marks above* denote that the enzyme(s) responsible is still unknown. *B*, schematic of the CoQ₆ biosynthetic pathway in yeast. The proposed function of Ptc7ₛ as a mitochondrial phosphatase modulating Coq7 activity is indicated. Ptc7ₙₛ has been localized to nuclear membrane. The *gray bars* represent the exon regions of the RNA, and the *thin gray line* represents the intron region of the RNA. The *pink-colored regions* represent the predicted 38-amino acid mitochondrial targeting sequence (*MTS*) of the protein, the *yellow region* represents the 31-amino acid intron of the protein (which interrupts the MTS after amino acid 19, hence spanning from amino acid 20 to 50), and the *blue region* depicts the mature and spliced polypeptide, which spans from amino acid 51 to 374 (47).

prenyl-4-hydroxybenzoic acid (HHB), an early CoQ₆ biosynthetic intermediate (Fig. 3, *B* and *D*). Consistent with the increased synthesis of CoQ₆ being a consequence of Ptc7 action, the *snf2Δ* yeast show significantly lower ratios of ¹³C₆-DMQ₆ level to ¹³C₆-CoQ₆ content, indicating a significant increase in the efficiency of conversion of DMQ₆ to CoQ₆, namely the step catalyzed by Coq7, a target of Ptc7ₛ (Fig. 3*C*) (11). Strikingly, we also observe that the levels of both steady-state and *de novo* synthesized HHB are significantly lower in *snf2Δ* than in the WT yeast (Fig. 3*D*). This suggests that the deletion of Snf2 not only causes higher CoQ₆ production by

regulating catalysis from DMQ₆ but that it also funnels the early precursors more efficiently than WT, thus allowing a more streamlined conversion of intermediates of the pathway to the overall product of CoQ₆. This is reinforced by the observation that *snf2Δ* yeast show significantly lower ratios of ¹³C₆-HHB to ¹³C₆-CoQ₆ content (Fig. 3*E*).

### Depletion of Snf2 during batch growth is associated with increased PTC7 splicing and increased CoQ₆ production

Because *snf2Δ* yeast have a significantly slower growth rate than WT, we considered the possibility that the increased CoQ₆
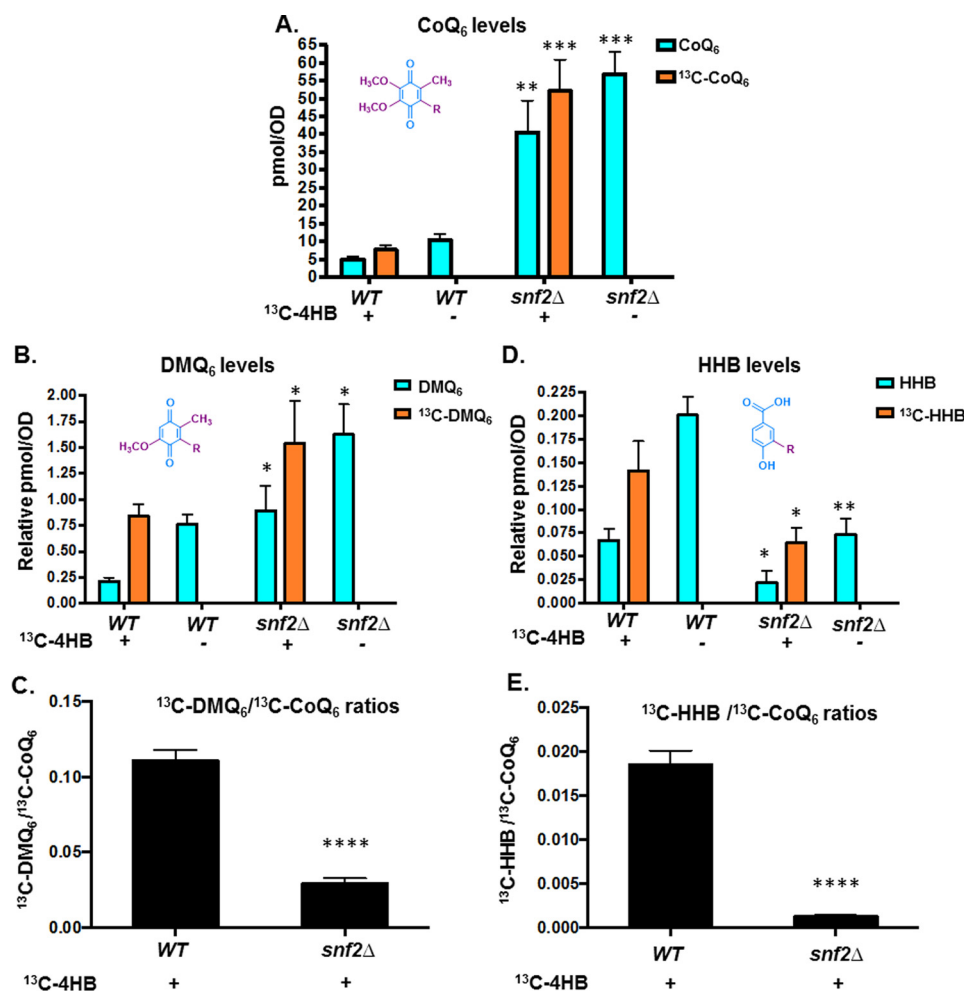
**Figure 3. Deletion of *SNF2* leads to increased steady state levels and *de novo* CoQ$_6$ biosynthesis in yeast and improves the flux from DMQ$_6$ to CoQ$_6$.**
*A*, levels of steady-state CoQ$_6$ ($^{12}$C-CoQ$_6$, *blue bars*) and *de novo* synthesized CoQ$_6$ ($^{13}$C$_6$-CoQ$_6$, *orange bars*) were determined in WT and *snf2*Δ yeast. $^{13}$C$_6$-4HB was added during midlog phase ($A_{600} = 0.5$), and labeling was allowed to proceed until a cell density of $A_{600} \sim 1.75$ was reached by both strains. $^{12}$C-CoQ$_6$ and $^{13}$C$_6$-CoQ$_6$ present in yeast cell pellets were quantified by HPLC-MS/MS, as described under "Experimental procedures." *Error bars*, S.D. of $n = 3$ biological replicates (unpaired Student's $t$ test between *corresponding bars* for *snf2*Δ and WT; **, $p < 0.005$; ***, $p < 0.0005$). *B*, levels of steady-state ($^{12}$C-DMQ$_6$, *blue bars*) and *de novo* synthesized DMQ$_6$ ($^{13}$C$_6$-DMQ$_6$, *orange bars*) were determined in WT and *snf2*Δ yeast. DMQ$_6$ was determined from the same cultures as in *A*. *Error bars*, S.D. of $n = 3$ biological replicates (unpaired Student's $t$ test between corresponding bars for *snf2*Δ and WT; *, $p < 0.05$). *C*, ratios of $^{13}$C$_6$-DMQ$_6$/$^{13}$C$_6$-CoQ$_6$ in WT and *snf2*Δ yeast, depicting flux of conversion of $^{13}$C$_6$-DMQ$_6$ to $^{13}$C$_6$-CoQ$_6$. *Error bars*, S.D. of $n = 3$ biological replicates (unpaired Student's $t$ test between corresponding bars for *snf2*Δ and WT; ****, $p < 0.00005$). *D*, levels of steady-state HHB ($^{12}$C-HHB, *blue bars*) and *de novo* synthesized HHB ($^{13}$C$_6$-HHB, *orange bars*) were determined in WT and *snf2*Δ yeast. HHB was determined from the same cultures as in *A*. *Error bars*, S.D. of $n = 3$ biological replicates (unpaired Student's $t$ test between *corresponding bars* for *snf2*Δ and WT; *, $p < 0.05$; **, $p < 0.005$). *E*, ratios of $^{13}$C-HHB/$^{13}$C-CoQ$_6$ in WT and *snf2*Δ yeast, depicting flux of conversion of $^{13}$C$_6$-HHB to $^{13}$C$_6$-CoQ$_6$. *Error bars*, S.D. of $n = 3$ biological replicates (unpaired Student's $t$ test between *corresponding bars* for *snf2*Δ and WT; ****, $p < 0.00005$).

synthesis was a consequence of the increased time in culture required to achieve equal cell density. To address this, rates of CoQ$_6$ biosynthesis in WT and *snf2*Δ yeast were determined at timed intervals of culture. First, measurements of steady-state and *de novo* synthesis rates of CoQ$_6$ between 2 and 12 h of batch growth in YPD revealed that whereas there is indeed an increased rate of synthesis in the *snf2*Δ yeast strain, the steady-state levels of CoQ$_6$ plateau within 4–6 h of labeling (Fig. 4*A*). We also observe decreasing levels of Snf2 as the time course progresses and nutrients are depleted (Fig. 4*B*). Consistent with the role of Snf2 in RPG transcription, RPG levels decrease with time in batch cultures of yeast, in a manner that tracks well with decreasing levels of Snf2 (Fig. 4*C*). This decrease also coincides with a concomitant increase in the splicing of *PTC7* (Fig. 4, *D* and *E*). Notably, splicing of the *PTC7* transcript in *snf2*Δ yeast starts off higher than in WT yeast, but as Snf2 is depleted

from the WT strain, splicing of the *PTC7* transcript approaches the levels of splicing in the *snf2*Δ strain (Fig. 4*F*).

To better understand the kinetics of CoQ$_6$ synthesis, a shorter time course was performed to capture points preceding the plateau, between 0 and 5 h of labeling. Within 4 h after labeling with $^{13}$C-4HB precursor, significant down-regulation in the levels of Snf2 protein is evident (Fig. 5*A*). The decrease in the level of Snf2 protein is mirrored in the increase in splicing efficiency of *PTC7* transcript in the WT strain (Fig. 5, *B–E*). It is interesting to note that the *PTC7* transcript is initially better spliced in the *snf2*Δ strain than in WT, but as the levels of Snf2 in the WT yeast decrease, splicing improves to a degree comparable with the *snf2*Δ strain (Fig. 5, *D* and compare *C* and *F*).

Additionally, there is a striking increase in the overall CoQ$_6$ product and its *de novo* biosynthesis in the *snf2*Δ yeast within 0–5 h of labeling, as compared with CoQ$_6$ levels of the WT
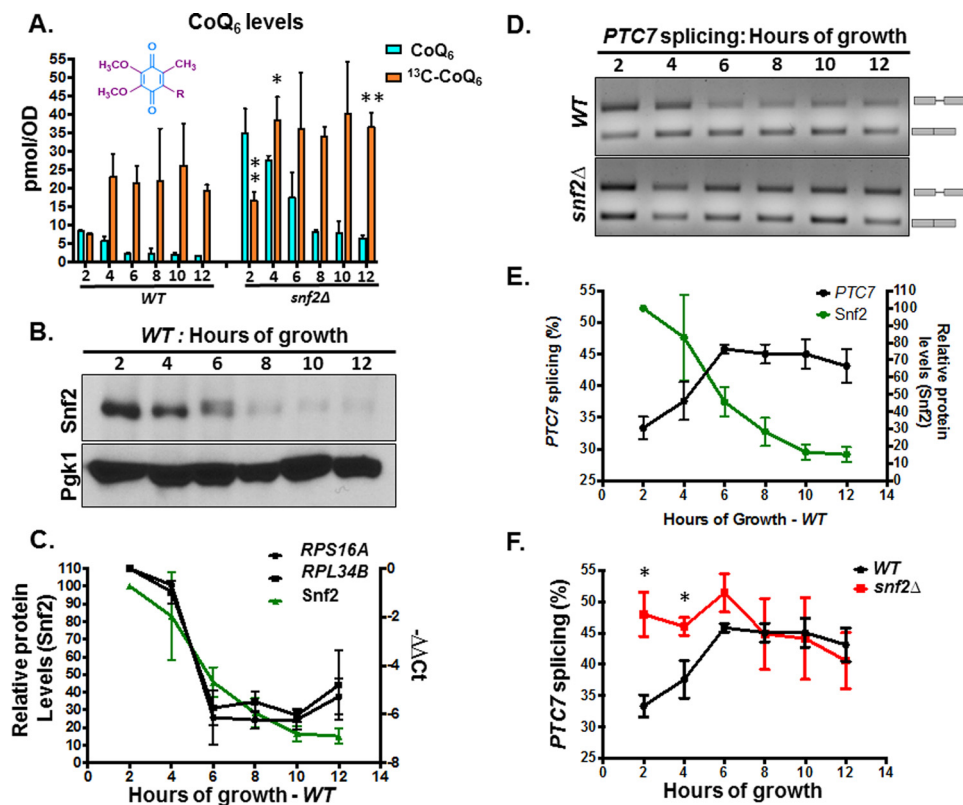
**Figure 4. Snf2 levels decrease during batch growth, coinciding with increased *PTC7* splicing and increased CoQ$_6$ synthesis.** *A*, levels of steady-state CoQ$_6$ ($^{12}$C-CoQ$_6$, *blue bars*) and *de novo* synthesized CoQ$_6$ ($^{13}$C$_6$-CoQ$_6$, *orange bars*) in WT and *snf2Δ* yeast were determined at the designated hours after labeling with $^{13}$C$_6$-4HB. *Error bars*, S.D. of *n* = 3 biological replicates (unpaired Student's *t* test between *corresponding bars* for *snf2Δ* and WT; *, *p* < 0.05; **, *p* < 0.005). *B*, steady-state levels of Snf2 protein in WT cells corresponding to samples from *A* were determined by immunoblot. Pgk1 served as a loading control. *C*, RT-qPCR measurement of selected intron-containing RPG transcripts (*black lines*) and Snf2 protein levels (*green line*) in WT yeast cells were determined at the designated hours after labeling with $^{13}$C$_6$-4HB as indicated in *A*. Shown is the mean of three biological replicates. *Error bars*, S.D. *D*, expression and splicing of *PTC7* in WT and *snf2Δ* yeast cells corresponding to samples from *A*. PCR products representing the spliced and nonspliced forms are indicated. *E*, quantification of splicing of *PTC7* transcript (*black line*) and Snf2 protein levels (*green line*) in WT yeast cells corresponding to samples from *D*. Snf2 protein levels were previously depicted in *C* and are shown here again for purposes of comparison. Shown is the mean of three biological replicates. *Error bars*, S.D. *F*, quantification of splicing of *PTC7* transcripts in WT and *snf2Δ* yeast cells corresponding to samples from *D*. The splicing of WT *PTC7* shown in *D* is depicted again here for purposes of comparison. Shown is the mean of three biological replicates. *Error bars*, S.D. (unpaired Student's *t* test; *, *p* < 0.05.)

during the same time course (Fig. 6, compare *A* and *F*). Furthermore, the gradual increase in CoQ$_6$ biosynthesis observed in the WT strain plateaus at 3–4 h after labeling (Fig. 6*A*), by which point the significant down-regulation in the levels of Snf2 protein is also evident (Fig. 5*A*). The steady-state and *de novo* synthesized levels of DMQ$_6$ and HHB were also measured in the 5-h time course of WT and *snf2Δ* yeast (Fig. 6, *B*, *C*, *G*, and *H*). Strikingly, the conversion of *de novo* DMQ$_6$ to CoQ$_6$ increases (as shown by the decreased ratio of $^{13}$C$_6$-DMQ$_6$ to $^{13}$C$_6$-CoQ$_6$) in a manner concurrent with the decrease in Snf2 levels and increase in *PTC7* splicing in WT (compare Fig. 6*D* with Fig. 5 (*A* and *B*)). In fact, as the levels of Snf2 in WT yeast decrease, the conversion efficiency of DMQ$_6$ to CoQ$_6$ approaches the low ratio of DMQ$_6$ to CoQ$_6$ in *snf2Δ* yeast (Fig. 6, compare *D* and *I*). The role of Ptc7$_s$ in the increased synthesis of CoQ$_6$ in the absence of Snf2 can be inferred from the observation that whereas the conversion efficiency from DMQ$_6$ to CoQ$_6$ is higher in the absence of Snf2, the level of DMQ$_6$ itself does not change appreciably between WT and *snf2Δ* yeast over the 5-h time course (Fig. 6, compare *B* and *G*). However, the *snf2Δ* cells also show significantly lower rates of HHB synthesis (Fig. 6, compare *C* and *H*), as well as lower ratios of $^{13}$C$_6$-HHB to $^{13}$C$_6$-CoQ$_6$ content (Fig. 6, compare *E* and *J*), consistent with

the observation that deletion of Snf2 markedly accelerates the synthesis of CoQ$_6$, presumably by expediting the conversion of these intermediates to the final product.

### RPG down-regulation in general leads to increased PTC7 splicing

Our previous work showed that Snf2-dependent down-regulation of ribosomal protein genes enhances splicing, particularly of genes with nonconsensus splice sites. To determine whether the observed increase in *PTC7* splicing is a consequence of RPG down-regulation *per se*, rapamycin was used to inhibit target of rapamycin (TOR)-dependent RPG transcription in a Snf2-independent manner (28) (Fig. 7*A*). It has also been previously published that rapamycin mitigates certain mitochondrial disorders in *Drosophila* and improves lifespan in response to TOR inhibition, purportedly by modulating carbon metabolism (29). In our work, rapamycin treatment led to a significant increase in the splicing of the *PTC7* transcript (Fig. 7, *B* and *C*). As previously observed, the change in the ratio of Ptc7$_s$/Ptc7$_{ns}$ protein (Fig. 1*D*) is greater than the change in the ratio of spliced to nonspliced transcript upon the deletion of Snf2 (Fig. 1*B*). This suggests that whereas Snf2-dependent RPG down-regulation changes the splicing of the *PTC7* transcript,
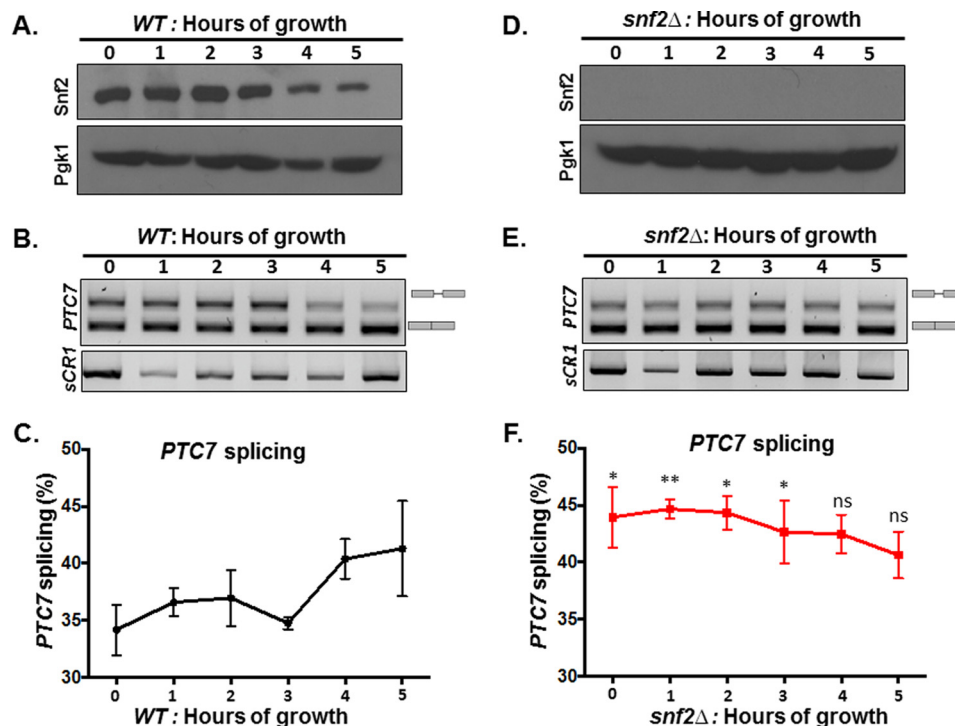
**Figure 5. The decrease in Snf2 levels over time in batch cultures of WT yeast correlates with enhanced splicing of *PTC7* RNA.** *A*, steady-state levels of Snf2 protein in WT cells corresponding to samples from indicated time points were determined by immunoblot. Pgk1 (phosphoglycerate kinase 1) served as a loading control. *B*, expression and splicing of *PTC7* in WT yeast cells corresponding to samples from *A*; PCR products represent the spliced and nonspliced forms, as indicated. *C*, quantification of splicing of *PTC7* transcript (*black line*) in WT yeast cells corresponding to samples from *B*. Shown is the mean of three biological replicates. *Error bars*, S.D. *D*, the Snf2 protein is absent in *snf2*Δ cells corresponding to samples from the indicated time points as determined by immunoblot. Pgk1 served as a loading control. *E*, expression and splicing of *PTC7* in *snf2*Δ yeast cells corresponding to samples from *D*; PCR products representing the spliced and nonspliced forms are indicated. *F*, quantification of splicing of *PTC7* transcript (*red line*) in *snf2*Δ yeast cells corresponding to samples from *E*. Shown is the mean of three biological replicates. *Error bars*, S.D. (unpaired Student's *t* test between *corresponding bars* for *snf2*Δ and WT in *C*; *, $p < 0.05$; **, $p < 0.005$).

there are probably additional layers of gene regulation that control the relative levels of the Ptc7$_s$ and Ptc7$_{ns}$ protein isoforms. Experiments probing these mechanisms are currently ongoing. Nonetheless, these results are consistent with a model whereby down-regulation of RPG expression redirects spliceosomes from these abundant transcripts to otherwise poorly spliced transcripts, such as *PTC7* (5, 6). In light of the role of Snf2 in RPG expression, changes in Snf2 levels allow fine-tuning of splicing in response to the cell's metabolic needs.

### Ptc7 isoforms have differing and opposing effects on CoQ$_6$ synthesis

The predicted structures of the two isoforms of Ptc7, Ptc7$_s$ and Ptc7$_{ns}$, have been modeled (Fig. 8, *A* and *B*). In fact, the Ptc7$_{ns}$ contains a transmembrane helix, encoded by the *PTC7* intron, which is capable of spanning the nuclear membrane. Overall, the presence of this transmembrane helix is not predicted to influence the folding of the rest of the protein, thus potentially retaining its phosphatase activity (Fig. 8).

To determine the effect of each Ptc7 isoform on CoQ$_6$ synthesis, we assayed CoQ$_6$ levels in cells expressing both forms of Ptc7, Ptc7$_s$ only, Ptc7$_{ns}$ only, or neither (*ptc7*Δ). As reported previously, there is no significant change in CoQ$_6$ synthesis levels in the *ptc7*Δ mutant (12, 30). However, exclusive expression of Ptc7$_s$ leads to an increase in CoQ$_6$ synthesis, whereas exclusive expression of Ptc7$_{ns}$ leads to a decrease in CoQ$_6$ synthesis (Fig. 9*A*). The relative RNA levels from each strain are shown (Fig. 9*B*). Moreover, there are no significant changes

observed in the protein levels of Snf2 or Coq7, the target of Ptc7 activity (Fig. 9*C*), in these strains. Whereas each of these isoforms was expressed within the endogenous context and from the endogenous *PTC7* promoter, protein levels of the Ptc7$_{ns}$ appeared to be increased relative to the other isoform (Fig. 9, *B* and *C*), perhaps due to a cellular feedback mechanism that increases expression or enhances stability of Ptc7$_{ns}$.

The steady-state and *de novo* synthesized levels of CoQ$_6$ were also measured in a 5-h time course with the yeast strains expressing either Ptc7$_{ns}$ or Ptc7$_s$. Both steady-state and *de novo* CoQ$_6$ biosynthesis are significantly lower in Ptc7$_{ns}$ strain than in the Ptc7$_s$ and in fact appear to be actively repressed, suggesting that the two isoforms of Ptc7 have differing and opposing effects on CoQ$_6$ biosynthesis (Fig. 9*D*). In addition, the exclusive presence of Ptc7$_s$ causes increased *de novo* biogenesis of $^{13}$C-CoQ$_6$ as compared with the exclusive presence Ptc7$_{ns}$ (Fig. 9*D*). Whereas the positive effect of Ptc7$_s$ on CoQ$_6$ biosynthesis is consistent with the mechanisms of Ptc7 action described previously, it is clear that Ptc7$_{ns}$ has a repressive effect on CoQ$_6$ biosynthesis (compare Ptc7$_{ns}$ and *ptc7*Δ in Fig. 9*A*). To begin to elucidate the mechanism of this repression, we assayed the mRNA transcript levels of genes encoding components of the CoQ$_6$ biosynthetic complex (*viz. COQ1–11* and *PTC7*). On average, there is little change in the expression of the complex upon deletion of Snf2 (Fig. 9, *G* and *H*) or with the exclusive expression of Ptc7$_s$ or *ptc7*Δ. However, exclusive expression of Ptc7$_{ns}$ is associated with pronounced down-regulation of every
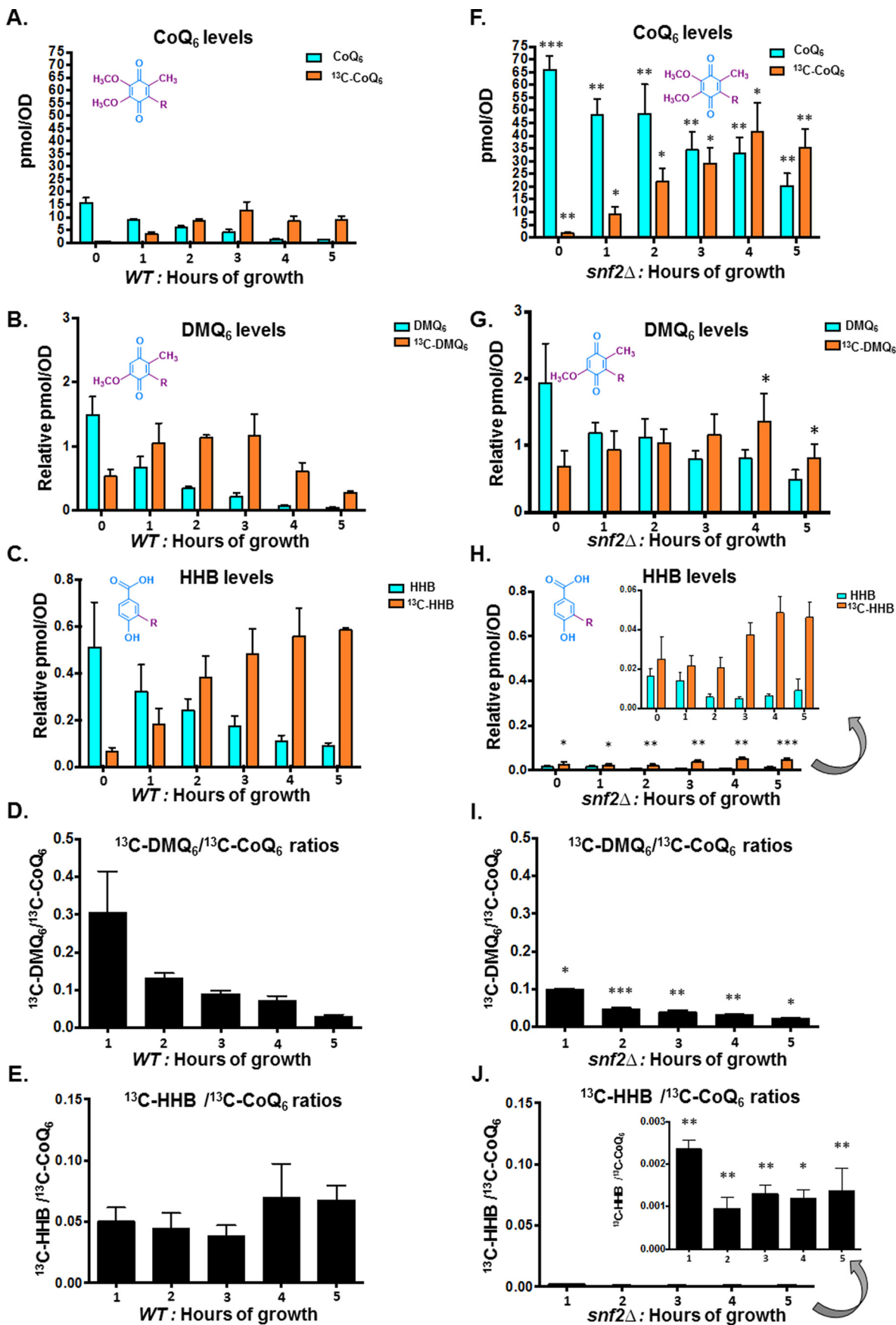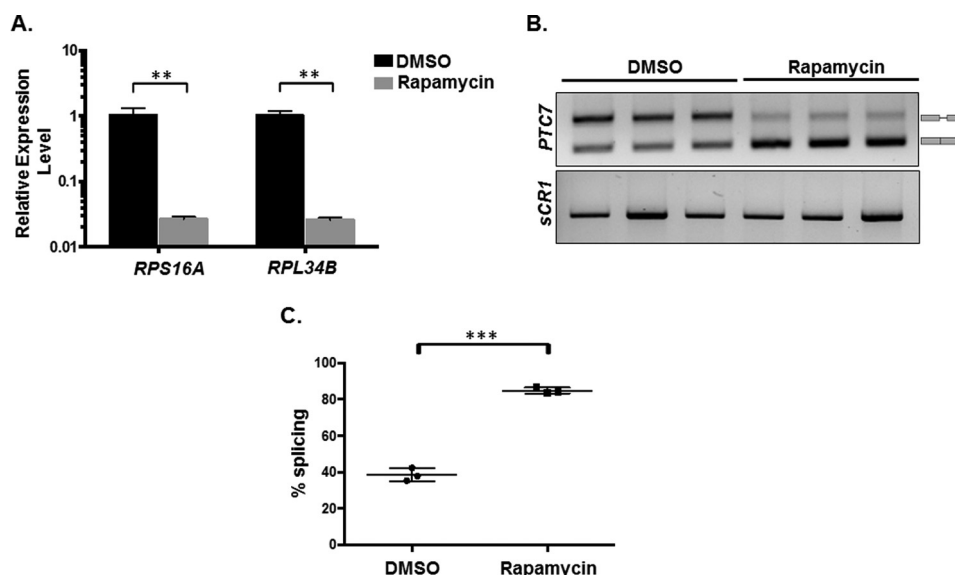
**Figure 7. RPG down-regulation and redistribution of spliceosomes result in increased *PTC7* splicing.** *A*, RT-qPCR measurement of selected intron-containing RPG transcripts between WT yeast treated with rapamycin and a vehicle control. Mean of three biological replicates (unpaired Student's *t* test, \*\**p* < 0.005). *Error bars*, S.D. *B*, expression and splicing of *PTC7* in WT yeast treated with rapamycin and a vehicle control (DMSO). PCR products representing the spliced and nonspliced forms are indicated. *C*, quantification of three independent biological replicates of *B* (unpaired Student's *t* test; \*\*\*, *p* < 0.0005). *Error bars*, S.D.

member of the CoQ-synthome (Fig. 9, *E* and *F*). Although the mechanism by which these components are down-regulated is unclear, it is interesting that Ptc7$_{ns}$ has previously been localized to the nuclear membrane (10), hinting at a novel role for this isoform in expression of the RNAs encoding the CoQ-synthome. Two possible mechanisms by which nucleus-localized Ptc7$_{ns}$ may affect synthesis of the CoQ-synthome are via direct action on nucleus-localized Coq7 or via indirect effects on gene expression. It is important to mention here that to the best of our knowledge, no reports have demonstrated nuclear localization of, or a nuclear role for, Coq7 in *S. cerevisiae*.

Interestingly, yeast strains engineered to express either Ptc7$_s$ or Ptc7$_{ns}$ still retain the ability to grow on medium containing a non-fermentable carbon source, as do *ptc7Δ* null mutants (data not shown). This is consistent with our prior observations that ~1–10% of CoQ$_6$ levels are sufficient for comparable growth on medium containing a nonfermentable carbon source. It has

been postulated that residual CoQ$_6$ levels are observed due to the overlapping activities of Ptc5 and/or Ptc6, and in fact the *ptc5Δptc7Δ* double null mutant has impaired growth under conditions of temperature stress (11, 31). It is also worth noting that unlike the deletion of *SNF2*, the conversion efficiencies or ratios between the early components of the pathway (DMQ$_6$ or HHB) and CoQ$_6$ do not vary between strains exclusively expressing either Ptc7 isoform (Fig. 10, *C* and *D*). This is because although there are significant changes in the levels of *de novo* synthesized DMQ$_6$ as well as HHB when comparing Ptc7$_s$ to Ptc7$_{ns}$ (Fig. 10, *A* and *B*), Ptc7$_s$ is synthesizing higher levels of *de novo* CoQ$_6$, DMQ$_6$, and HHB, compared with overall lower levels of these same lipids in Ptc7$_{ns}$ (Fig. 10, *C* and *D*). Thus, the overall conversion efficiencies (ratios) between both isoforms are comparable (Fig. 10, *C* and *D*). This is consistent with our interpretation that the absence of Snf2 contributes to the metabolic state of the cell in other ways in addition to its role in regulation of the Ptc7 isoforms.

**Figure 6. Overall conversion efficiency of the CoQ$_6$ biosynthetic pathway increases upon depletion of Snf2, with increased conversions of both DMQ$_6$ to Q$_6$ and HHB to Q$_6$.** *A*, levels of steady-state CoQ$_6$ ($^{12}$C-CoQ$_6$, *blue bars*) and *de novo* synthesized CoQ$_6$ ($^{13}$C$_6$-CoQ$_6$, *orange bars*) in WT yeast cells were determined at the designated hours after labeling with $^{13}$C$_6$-4HB. *Error bars*, S.D. of *n* = 3 biological replicates. *B*, levels of steady-state DMQ$_6$ ($^{12}$C-DMQ$_6$, *blue bars*) and *de novo* synthesized DMQ$_6$ ($^{13}$C$_6$-DMQ$_6$, *orange bars*) in WT yeast were determined at the designated hours after labeling with $^{13}$C$_6$-4HB. *Error bars*, S.D. of *n* = 3 biological replicates. *C*, levels of steady-state HHB ($^{12}$C-HHB, *blue bars*) and *de novo* synthesized ($^{13}$C$_6$-HHB, *orange bars*) in WT and *snf2Δ* yeast were determined at the designated hours after labeling with $^{13}$C$_6$-4HB. *Error bars*, S.D. of *n* = 3 biological replicates. *D*, the ratio of $^{13}$C$_6$-DMQ$_6$/$^{13}$C$_6$-CoQ$_6$ in WT yeast was determined at the designated hours after labeling with $^{13}$C$_6$-4HB. *Error bars*, S.D. of *n* = 3 biological replicates. The 0-h time point is excluded, because the ratio is not indicative of pathway conversion. *E*, the ratio of $^{13}$C$_6$-HHB/$^{13}$C$_6$-CoQ$_6$ in WT yeast was determined at the designated hours after labeling with $^{13}$C$_6$-4HB. *Error bars*, S.D. of *n* = 3 biological replicates. The 0-h time point is excluded, because the ratio is not indicative of pathway conversion. *F*, levels of steady-state CoQ$_6$ ($^{12}$C-CoQ$_6$, *blue bars*) and *de novo* synthesized ($^{13}$C$_6$-CoQ$_6$, *orange bars*) in *snf2Δ* yeast cells were determined at the designated hours after labeling with $^{13}$C$_6$-4HB. *Error bars*, S.D. of *n* = 3 biological replicates (unpaired Student's *t* test between *corresponding bars* for *snf2Δ* and WT in *A*; \*, *p* < 0.05; \*\*, *p* < 0.005; \*\*\*, *p* < 0.0005). *G*, levels of steady-state DMQ$_6$ ($^{12}$C-DMQ$_6$, *blue bars*) and *de novo* synthesized DMQ$_6$ ($^{13}$C$_6$-DMQ$_6$, *orange bars*) in *snf2Δ* yeast were determined at the designated hours after labeling with $^{13}$C$_6$-4HB. *Error bars*, S.D. of *n* = 3 biological replicates. (unpaired Student's *t* test between *corresponding bars* for *snf2Δ* and WT in *B*; \*, *p* < 0.05). *H*, levels of steady-state HHB ($^{12}$C-HHB, *blue bars*) and *de novo* synthesized HHB ($^{13}$C$_6$-HHB, *orange bars*) in *snf2Δ* yeast were determined at the designated hours after labeling with $^{13}$C-4HB. *Error bars*, S.D. of *n* = 3 biological replicates (unpaired Student's *t* test between corresponding bars for *snf2Δ* and WT in *C*; \*, *p* < 0.05; \*\*, *p* < 0.005; \*\*\*, *p* < 0.0005). *I*, the ratio of $^{13}$C$_6$-DMQ$_6$/$^{13}$C$_6$-CoQ$_6$ in *snf2Δ* yeast cells was determined at the designated hours after labeling with $^{13}$C$_6$-4HB. *Error bars*, S.D. of *n* = 3 biological replicates (unpaired Student's *t* test between corresponding bars for *snf2Δ* and WT in *D*; \*, *p* < 0.05; \*\*, *p* < 0.005; \*\*\*, *p* < 0.0005). The 0-h time point is excluded, because the ratio is not indicative of pathway conversion. *J*, the ratio of $^{13}$C$_6$-HHB/$^{13}$C$_6$-CoQ$_6$ in *snf2Δ* yeast cells was determined at the designated hours after labeling with $^{13}$C$_6$-4HB. *Error bars*, S.D. of *n* = 3 biological replicates (unpaired Student's *t* test between *corresponding bars* for *snf2Δ* and WT in *E*; \*, *p* < 0.05; \*\*, *p* < 0.005). The 0-h time point is excluded, because the ratio is not indicative of pathway conversion.
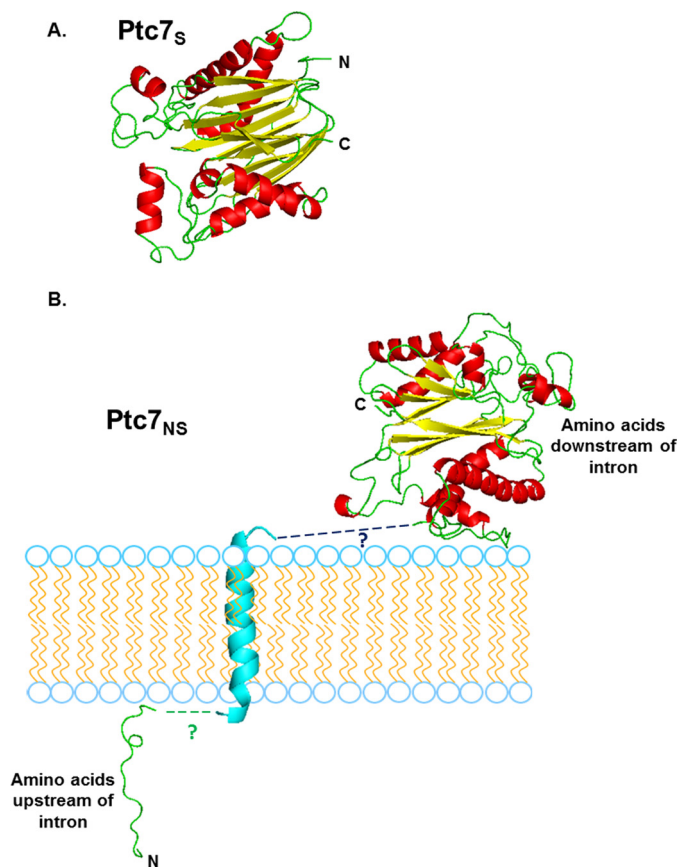
**Figure 8. Structural predictions of mitochondrial Ptc7ₛ and nuclear membrane traversing Ptc7ₙₛ.** *A*, PHYRE2 homology modeling of mature mitochondrial Ptc7ₛ, which is experimentally determined to start at amino acid Gly³⁹ (46). 85% of residues modeled at >90% confidence (15% of residues modeled *ab initio*). The N terminus and C terminus of the protein are shown. *B*, PHYRE2 homology modeling of nuclear membrane Ptc7ₙₛ. The predicted trans-membrane helix encoded by the intron is shown in *cyan*. 86% of residues modeled at >90% confidence (14% of residues modeled *ab initio*. To show the interaction with the nuclear membrane, the N-terminal loop residing on the one side of the nuclear membrane is proposed to be linked to the modeled transmembrane helix, which is then proposed to be linked to the rest of the Ptc7 protein that is predicted to reside on the alternate side of the nuclear membrane. The *nine black dashes* connecting the helix to the larger portion of the protein represent nine amino acids in the intron that were in an unmodeled region.

These data reveal a novel role for Snf2 in respiration and specifically in the transition from a largely fermentative mode of metabolism to a largely respiratory one in *S. cerevisiae*, as shown by the model in Fig. 11. Under conditions of high nutrient availability, Snf2-dependent transcription of intron-rich RPGs sequesters spliceosomes away from transcripts with weak splice sites, such as *PTC7.* As a consequence, both isoforms of the Ptc7 protein are expressed at appreciable levels, and their opposing effects on CoQ₆ synthesis ensure that CoQ₆ is maintained at a relatively low level. As the nutrients in the medium are depleted, the levels of Snf2 and, consequently, RPG transcripts, decrease concurrently, freeing up spliceosomes to act on *PTC7.* This leads to better splicing of *PTC7* and a shift in the relative abundances of the two protein isoforms, which eventually leads to an increase in CoQ₆ synthesis.

## Discussion

Whereas it has been broadly acknowledged that chromatin states and chromatin factors influence splicing outcomes in

various organisms, identifying the functional importance of such regulation under biologically relevant conditions remains a challenge. We have shown previously that down-regulation of Snf2, the core ATPase component of the SWI/SNF chromatin-remodeling complex, in response to nutrient depletion leads to a change in cellular splicing outcomes due to down-regulation of RPGs and subsequent redistribution of spliceosomes (5, 6). We show here that Snf2-dependent changes in splicing of *PTC7* during yeast growth, combined with the general conditions in the cell in the absence of Snf2, causes a shift in the ratio of two distinct isoforms of the Ptc7 protein that have distinct and opposing effects on CoQ₆ biosynthesis. This change in the ratio of the isoforms is concomitant with an increase in CoQ₆ levels in the cell, preparing for the transition from a largely fermentative to a respiratory mode of metabolism.

Previous studies have presented contradictory evidence regarding the involvement of *PTC7* in CoQ₆ biosynthesis. Ptc7 is required for the dephosphorylation of Coq7, thus transitioning Coq7 to its "active" form, which is able to catalyze the penultimate step of the CoQ₆ pathway. This led to the prediction that the *ptc7*Δ strain would demonstrate decreased CoQ₆ synthesis, as assayed by quantification of lipids from purified mitochondria (11). Surprisingly, although Ptc7 supports general respiratory function, the absence of *PTC7* does not lead to a deficiency in CoQ₆ levels, as assayed in lipid extracts of whole cells (12) (Fig. 9*A*). The studies here help to resolve this apparent contradiction. Studies with the *ptc7*Δ cells fail to address the opposing roles that the two Ptc7 isoforms have in the cell under WT conditions. Only cells with the capacity to express both Ptc7ₛ and Ptc7ₙₛ can accurately reflect the full extent of Ptc7 function. We demonstrate that exclusive expression of Ptc7ₙₛ has a significant repressive effect on CoQ₆ biosynthesis (Fig. 9, *A* and *D*). Notably, the rates of conversions from precursors in the pathway to the final product remained unchanged, indicating down-regulation of the entire pathway (Fig. 10, *C* and *D*). Consistent with this, we observe down-regulation of almost all of the components of the CoQ₆ biosynthetic complex upon exclusive expression of Ptc7ₙₛ (Fig. 9*F*). The mechanism by which Ptc7ₙₛ affects RNA expression is as yet unknown, and investigations to understand the same are ongoing.

*PTC7* is not the only known example of a gene in *S. cerevisiae* encoding functional proteins from both the nonspliced pre-mRNA as well as the "mature" spliced mRNA (10). We recently reported translation of unspliced *GCR1* pre-mRNA leading to a functional Gcr1 protein, although in this case, translation starts from within the retained intron (7). Whereas the read-through nature of the intron is conserved across most *Saccharomycetaceae* species, the intron is excised in the same species (analysis of publicly available RNA-seq data sets; data not shown), rendering it likely that both forms of the protein are necessary and functional. This is illustrated in the case of *Tetrapisispora blattae*, which, like *S. cerevisiae*, underwent a whole genome duplication event; but unlike *S. cerevisiae*, which lost the duplications of most of its genes, *T. blattae* retains two copies of the *PTC7* gene. Interestingly, the two *PTC7* genes in *T. blattae* subfunctionalized into a gene that encodes a mitochondrial PP2C (Ptc7ᵦ, from a spliced transcript of *PTC7b* con-
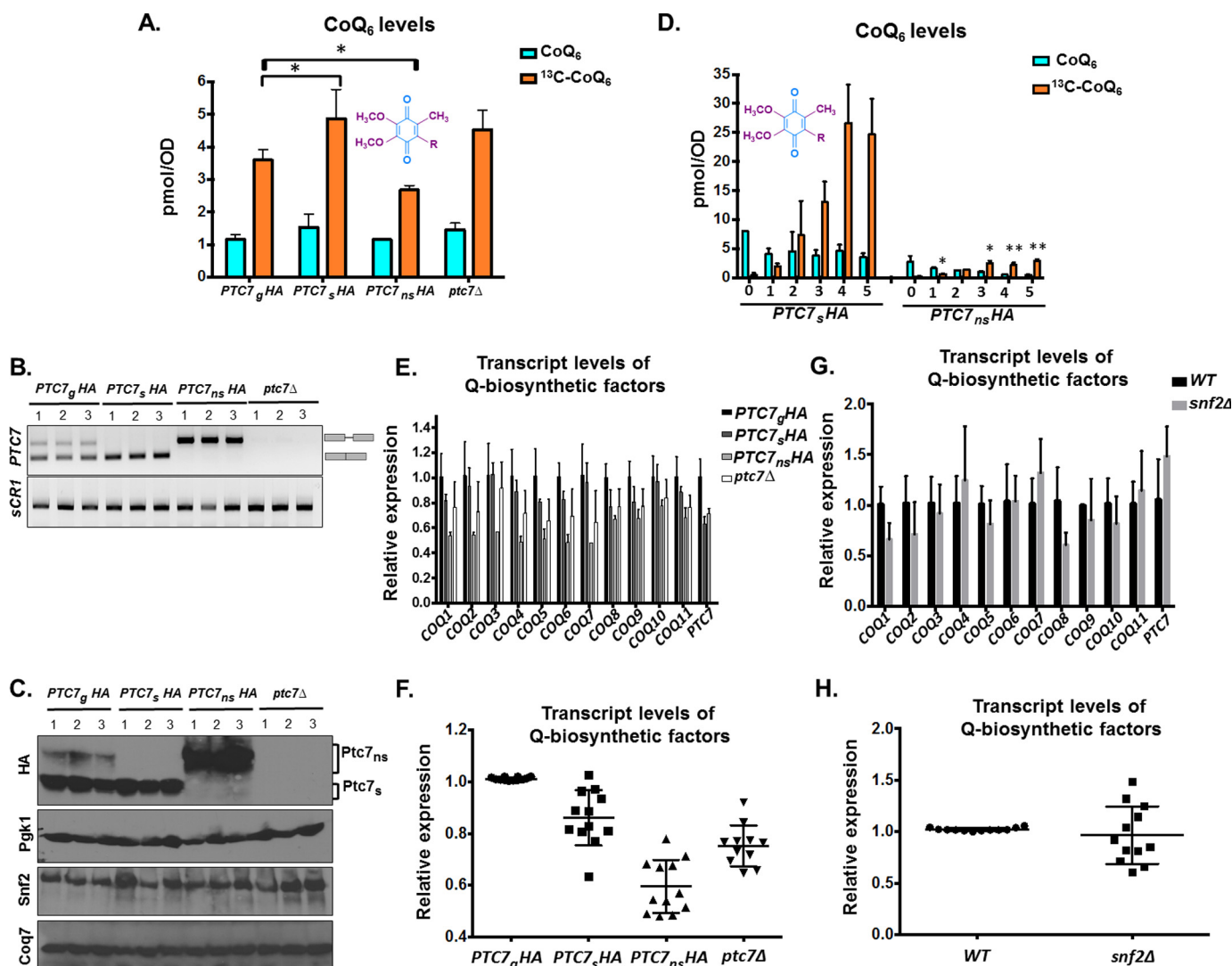
**Figure 9. Ptc7 isoforms have differing and opposing effects on CoQ_6 synthesis.** *A*, levels of steady-state CoQ_6 ($^{12}$C-CoQ_6, *blue bars*) and *de novo* synthesized CoQ_6 ($^{13}$C_6-CoQ_6, *orange bars*) in strains expressing distinct Ptc7 isoforms (*PTC7_gHA*, genomic, both isoforms expressed; *PTC7_sHA*, exclusively expresses the isoform from spliced mRNA; *PTC7_nsHA*, exclusively expresses the isoform from nonspliced pre-mRNA) and *ptc7Δ*. Labeling with $^{13}$C_6-4HB was allowed to proceed for 3 h. *Error bars*, S.D. of $n = 3$ biological replicates (unpaired Student's *t* test; *, $p < 0.05$). *B*, expression and splicing of *PTC7* for samples corresponding to *A*. PCR products representing the spliced and nonspliced forms are indicated. *C*, steady-state levels of HA-tagged Ptc7 proteins were determined by immunoblotting for samples corresponding to *A*. Proteins derived from the nonspliced and spliced forms of the *PTC7* RNA are denoted as Ptc7_ns and Ptc7_s, respectively. Pgk1 (phosphoglycerate kinase 1) served as a loading control. Immunoblots for Snf2 and Coq7 are also included. *D*, levels of steady-state ($^{12}$C-CoQ_6, *blue bars*) and *de novo* synthesized ($^{13}$C_6-CoQ_6, *orange bars*) CoQ_6 in *PTC7_sHA* and *PTC7_nsHA* yeast cells were determined at the designated hours after labeling with $^{13}$C_6-4HB. *Error bars*, S.D. of $n = 3$ biological replicates (unpaired Student's *t* test between corresponding bars for *PTC7_sHA* and *PTC7_nsHA*; *, $p < 0.05$; **, $p < 0.005$). *E*, RT-qPCR measurement of *COQ1–COQ11* and *PTC7* transcript levels between strains expressing different Ptc7 isoforms (*PTC7_gHA*, genomic, both isoforms expressed; *PTC7_sHA*, exclusively expresses the isoform from spliced mRNA; *PTC7_nsHA*, exclusively expresses the isoform from nonspliced pre-mRNA) and *ptc7Δ*. Shown is the mean of three biological replicates. *Error bars*, S.D. *F*, summary analysis of transcript levels of Q-biosynthetic factors from *E*. *G*, RT-qPCR measurement of *COQ1-COQ11* and *PTC7* transcript levels between WT and *snf2Δ* yeast. Shown is the mean of three biological replicates. *Error bars*, S.D. *H*, summary analysis of transcript levels of Q-biosynthetic factors from *G*.

taining a stop codon within its intron) and a second gene encoding a PP2C predicted to localize to the nuclear envelope (Ptc7_a, from an nonspliced transcript of *PTC7a* (32). This conservation further suggests that both protein isoforms derived from the *PTC7* transcript in *S. cerevisiae* are functional. Cells lacking Ptc7_ns show increased sensitivity to latrunculin A treatment, compared with strains expressing both isoforms of Ptc7 or lacking Ptc7_s (10). Such sensitivity might suggest a distinct role for Ptc7_ns in actin filament formation.

It is noteworthy that nuclear roles for numerous metabolic enzymes have been described previously. The ability of metabolic enzymes to "moonlight" in the nucleus, affecting gene regulation at various steps, appears to be crucial for the ability of cells to sense and adapt to their potentially distinct nutrient environments (33). Numerous mitochondrial enzymes, such as succinate dehydrogenase, fumarase, aconitase, and malate dehydrogenase (all components of the Krebs cycle), have been shown to have significant nuclear roles in the regulation of gene expression (34–38). In some of these cases, enzymatic activity of these enzymes has been shown to be crucial to their nuclear roles (39). This precedence, combined with the evolutionarily conserved presence of an isoform of Ptc7 in the nuclear membrane, raises the possibility that a nucleus-localized phosphatase is crucial to regulation of components of the CoQ_6 biosyn-
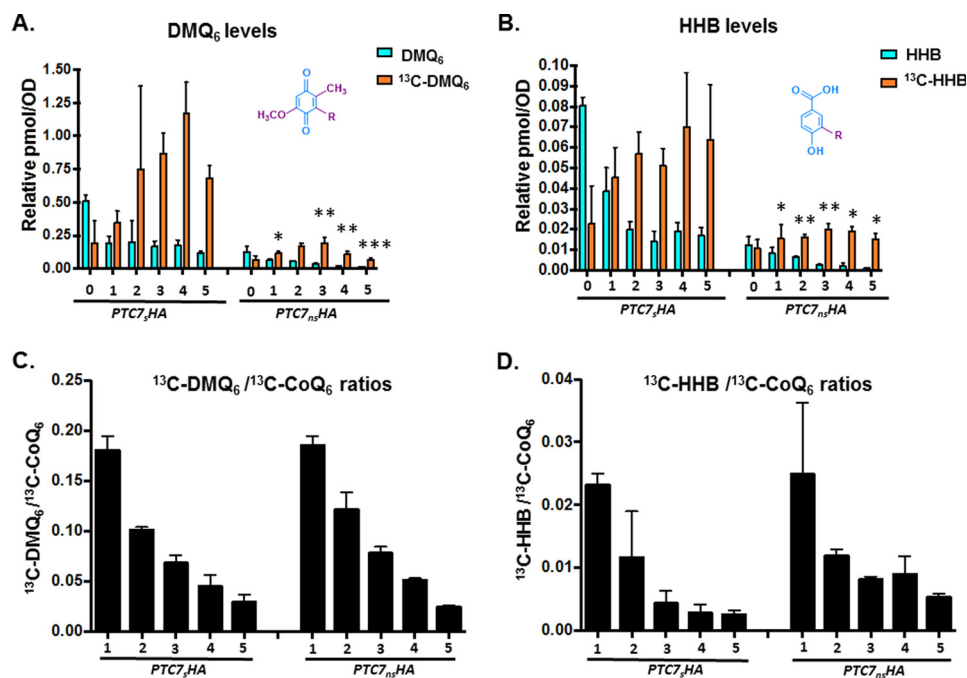
**Figure 10. Exclusive expression of Ptc7 isoforms dramatically alters levels of CoQ$_6$ biosynthetic pathway intermediates DMQ$_6$ and HHB, yet overall conversion efficiency between both isoforms is comparable.** *A*, levels of steady-state DMQ$_6$ ($^{12}$C-DMQ$_6$, *blue bars*) and *de novo* synthesized DMQ$_6$ ($^{13}$C$_6$-DMQ$_6$, *orange bars*) in *PTC7$_s$HA* and *PTC7$_{ns}$HA* yeast cells were determined at the designated hours after labeling with $^{13}$C$_6$-4HB. *Error bars*, S.D. of *n* = 3 biological replicates (unpaired Student's *t* test between *corresponding bars* for *PTC7$_s$HA* and *PTC7$_{ns}$HA*; *, $p < 0.05$; **, $p < 0.005$; ***, $p < 0.0005$). *B*, levels of steady-state HHB ($^{12}$C-HHB, *blue bars*) and *de novo* synthesized HHB ($^{13}$C$_6$-HHB, *orange bars*) in *PTC7$_s$HA* and *PTC7$_{ns}$HA* yeast cells were determined at the designated hours after labeling with $^{13}$C$_6$-4HB. *Error bars*, S.D. of *n* = 3 biological replicates (unpaired Student's *t* test between *corresponding bars* for *PTC7$_s$HA* and *PTC7$_{ns}$HA*; *, $p < 0.05$; **, $p < 0.005$). *C*, ratio of $^{13}$C$_6$-DMQ$_6$/$^{13}$C$_6$-CoQ$_6$ in *PTC7$_s$HA* and *PTC7$_{ns}$HA* yeast cells were determined at the designated hours after labeling with $^{13}$C$_6$-4HB. Ratios were derived from levels of $^{13}$C$_6$-CoQ$_6$, as shown in Fig. 7*D*. *Error bars*, S.D. of *n* = 3 biological replicates. The 0-h time point is excluded, because the ratio is not indicative of pathway conversion. *D*, ratio of $^{13}$C$_6$-HHB/$^{13}$C$_6$-CoQ$_6$ in *PTC7$_s$HA* and *PTC7$_{ns}$HA* yeast cells were determined at the designated hours after labeling with $^{13}$C$_6$-4HB. Ratios were derived from levels of $^{13}$C$_6$-CoQ$_6$, as shown in Fig. 7*D*. *Error bars*, S.D. of *n* = 3 biological replicates. The 0-h time point is excluded, because the ratio is not indicative of pathway conversion.

thetic pathway. Intriguingly, CLK-1 and COQ7, the *C. elegans* and human homologs of Coq7, which is a target for Ptc7 in *S. cerevisiae* (11), have been demonstrated to localize to the nucleus and are postulated to have roles independent of CoQ biosynthesis (40). COQ7 has also been shown to associate with chromatin in HeLa cells (40), although recently this has been attributed to a transformed cell phenomenon (41). Whereas nuclear localization of Coq7 in *S. cerevisiae* has not been demonstrated, we suggest a potential role in nuclear gene regulation for Ptc7 via phosphatase activity on Coq7 or other unidentified targets, including conventionally nuclear and other "moonlighting" mitochondrial enzymes.

It is also possible that Ptc7 has a substrate other than Coq7 that affects expression of the CoQ$_6$-synthome. In fact, a recent study identified with high confidence numerous differentially phosphorylated proteins in a *ptc7Δ* strain (12). Notably, this proteomic analysis does not distinguish between the potential effects of the two Ptc7 isoforms globally. In fact, rescue using plasmid-based expression of *PTC7* (full-length) does not restore dephosphorylation levels for a number of nuclear proteins, although the increased phosphorylation of mitochondrial proteins upon deletion of *PTC7* is almost completely reversed by exogenous expression of Ptc7 (12). Furthermore, it is possible that the mitochondrial role for Ptc7$_s$ is in fact covered by multiple redundancies. Ptc5 and Ptc6, two other PP2C protein phosphatases, also localize to the mitochondrial membrane, and *PTC5* demonstrates a negative genetic interaction with

*PTC7*, indicating the possibility of overlapping functions (11, 31).

Interestingly, the effect of Snf2 deletion on CoQ$_6$ biosynthesis does not perfectly mirror the exclusive expression of Ptc7$_s$. We postulate that this is partially due to the Snf2 affecting the flux of the entire CoQ$_6$ biosynthetic pathway, as demonstrated by the increased conversion of early precursors. Whereas deletion of Snf2 does not, on average, change the expression of the components of the CoQ$_6$-synthome (Fig. 9, *G* and *H*), it is possible the Snf2 may have other effects of CoQ$_6$ flux. We are exploring these possibilities.

Intriguingly, although the absence of Snf2 enhances levels of CoQ$_6$, yeast strains lacking Snf2 have a severe growth defect on non-fermentable carbon sources, such as glycerol or acetate (26) (Fig. 1*E*). However, Snf2 protein is undetectable by immunoblotting during growth in medium containing glycerol or acetate as the only carbon source (data not shown). This leads us to hypothesize that before Snf2 protein is down-regulated in response to glucose depletion, it is required for the transition from a fermentative metabolic state to one that is predominantly respiratory in nature. The molecular details of the requirement for Snf2 in this transition are the subject of ongoing investigation. However, it is probably at least in part due to its reported role in the activation (de-repression) of genes whose transcription had previously been subject to glucose-mediated catabolite repression. This activation occurs once the glucose has been depleted or the yeast have been shifted to a
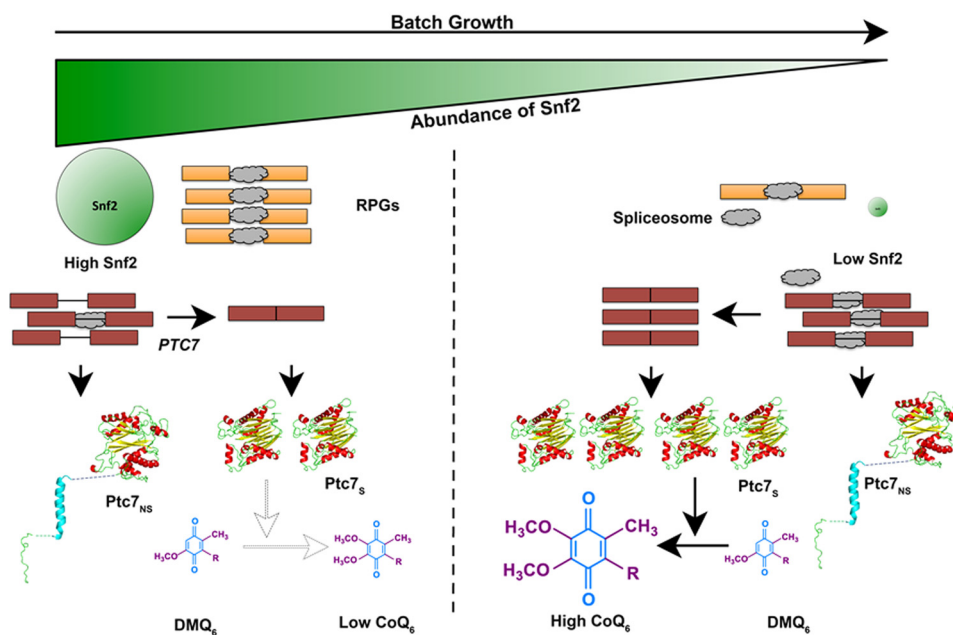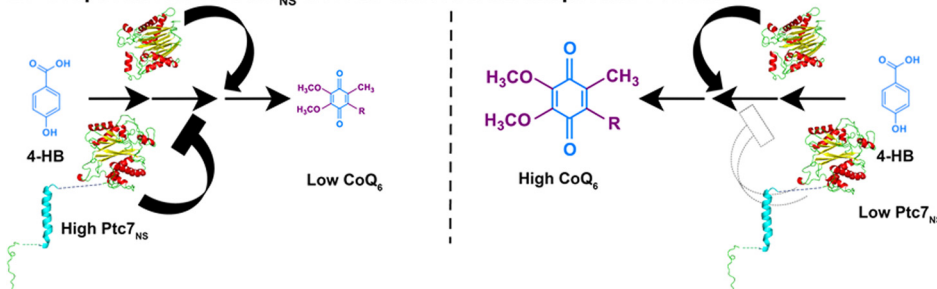
**A. Snf2 regulates the relative abundance of Ptc7 isoforms to control CoQ$_6$ synthesis.**



**B. Proposed role for Ptc7$_{NS}$ isoform derived from unspliced *PTC7* RNA.**



**Figure 11. Model for a novel role for Snf2 in respiration, and in the transition from a primarily fermentative mode of metabolism to a primarily respiratory mode of metabolism.** *A*, during *S. cerevisiae* batch growth, the abundance of Snf2 decreases in conjunction with depletion of nutrients in the medium. RPGs under the control of Snf2 are down-regulated, allowing redistribution of spliceosomes to other poorly spliced transcripts. Splicing of the *PTC7* transcript increases, enhancing the ratio of Ptc7$_s$/Ptc7$_{ns}$ and overall levels of Ptc7$_s$. These changes in Ptc7 isoform levels lead to increased conversion of DMQ$_6$ and increased synthesis of CoQ$_6$. The *darker arrow* represents a greater effect or reaction conversion, whereas a *lighter arrow* represents a smaller effect or reaction conversion. *B*, Ptc7$_{ns}$ has a repressive effect on CoQ$_6$ biosynthesis. CoQ$_6$ levels are low or high, depending on the levels of the Ptc7$_{ns}$ isoform relative to Ptc7$_s$. Similar to *A*, *darker arrows* and *bars* denote a larger effect, whereas *lighter arrows* and *bars* denote a smaller effect.

different, non-fermentable carbon source (26). We postulate that once the gene expression profile required for adaptation to the new nutrient environment has been initiated and/or established, the requirement for Snf2 is relieved, and in fact, the down-regulation of Snf2 enhances splicing of *PTC7*. This transient requirement for Snf2 bears striking similarities to a previous report detailing the role of Snf2 in reversing Ume6-mediated repression at certain meiotic genes early in meiosis, before it is itself down-regulated to enable splicing of meiotic transcripts (6).

This work reveals a mechanism by which SWI/SNF acts as a nexus point in the fermentation–respiratory transition in *S. cerevisiae*. We also demonstrate opposing effects of isoforms of a single gene, *PTC7*, on the process of CoQ$_6$ biosynthesis, via distinct mechanisms. Numerous aspects of these mechanisms remain to be studied, as well as their potential roles in the gene regulation response to other physiological conditions that yeast might experience.

## Experimental procedures

### Yeast strains and culture conditions

The yeast strains used in this study are listed in Table 1. All strains except W303Δcoq2 are derived from the BY background. Yeast strains were grown in YPD (1% yeast extract, 2% peptone, 2% dextrose) medium at 30 °C. Snf2 and Ptc7 null strains were maintained with a backup expression plasmid (pRS316 backbone harboring either *SNF2* or *PTC7*). The plasmid was shuffled out by growth on 5-fluoroorotic acid before using the strains in experiments. Strains with tagged isoforms of Ptc7 were a kind gift from Dr. Ron Davis (10). These strains were back-crossed against WT or *snf2*Δ strains, and daughter strains used for this study are listed in Table 1. The *snf2*Δ strain was observed to spontaneously mutate if grown on YPD for longer than 7–8 days, acquiring suppressor mutations that made it difficult to distinguish from WT. Hence, for all experiments with *snf2*Δ, the plasmid contain-

**Table 1**
Genotype and source of yeast strains

| Strain number | Name | Genotype | Source/reference |
|---|---|---|---|
| TJY6724 | WT | *MATa his3Δ leu2Δ LYS2 met15Δ ura3Δ* | Ref. 6 |
| TJY6727 | *snf2Δ* | *MATα his3Δ leu2Δ ura3Δ snf2Δ::NatMX* | Ref. 6 |
| TJY7114 | *PTC7$_g$HA* | *MATa his3Δ leu2Δ ura3Δ PTC7$_g$HA:KanMX* | This study |
| TJY7115 | *snf2ΔPTC7$_g$HA* | *MATa his3Δ leu2Δ ura3Δ snf2Δ::NatMX PTC7$_g$HA:KanMX* | This study |
| W303Δ*coq2* | *coq2Δ* | *MATa ade2-1 his3-1,15 leu2-3,112 trp1-1 ura3-1 coq2::HIS3* | Ref. 47 |
| TJY7116 | *PTC7$_g$HA* | *MATa his3Δ leu2Δ ura3Δ PTC7$_g$HA:KanMX* | This study |
| TJY7118 | *PTC7$_{ns}$HA* | *MATa his3Δ leu2Δ ura3Δ PTC7$_{ns}$HA:KanMX* | This study |
| TJY7142 | *ptc7Δ* | *MATa his3Δ leu2Δ ura3Δ ptc7Δ:KanMX* | This study |
| BY4741Δ*coq9* | *coq9Δ* | *MATα his3Δ0 leu2Δ0 met15Δ0 ura3Δ0 coq9::KANMX4* | Ref. 48 |

ing *SNF2* was shuffled out prior to each experiment, allowing a fresh *snf2Δ* strain with each experiment, to avoid these suppressor mutants. We found that this was absolutely instrumental to observe the proper phenotype and behavior of the *snf2Δ* strain.

### RNA-sequencing analyses

The RNA-sequencing data reported in this study were generated previously (6). Briefly, RNA sequencing libraries were prepared using the Illumina Truseq® V3 kit and ribosomal RNA depletion (Ribo-Zero, Illumina). Single-end, 50-nucleotide sequence reads (HiSeq 2000) were aligned to SacCer3 and spliced transcripts from the Ares Lab Yeast Intron Database version 3 (42) in a single step using STAR (43). Only the highest scoring alignments for each read were kept, allowing for at most a single tie. Reads/kb/million were computed for each gene by dividing the total number of reads that aligned entirely within the gene's exon boundaries by the gene's total exon length in kilobase pairs per million mapped reads. Reads within ICGs were categorized as exonic, spliced, or unspliced. Exonic reads map entirely within an exon, as defined by the Ares Lab Yeast Intron Database. Introns with annotated small nucleolar RNAs within the defined intron boundaries were disregarded in this analysis. Spliced reads are those that align with a gap that corresponds to an annotated intron, and unspliced reads map partially within an exon and partially within an intron with no gap. Spliced and unspliced read counts were normalized by dividing total spliced counts by the number of potential unique alignment positions that contribute to the total. For spliced reads, this is read length minus one for every intron. For unspliced read counts, this is the length of the intron plus the read length minus one. Splicing efficiency for each intron was calculated as normalized spliced counts divided by the sum of the normalized spliced and normalized unspliced counts. Changes in splicing efficiency were calculated as percentage difference over WT efficiency and plotted against expression levels (reads/kb/million) in WT. Data are available under GEO accession number GSE94404, and detailed methods were described previously (6).

### RT-PCR and real-time PCR analysis

RNA was isolated from a 5-ml aliquot of cell culture corresponding to time points described in each experiment. After DNase treatment (Roche Applied Science), equal quantities of total RNA from each sample were used to make cDNA using a cDNA synthesis kit (Fermentas). To detect *PTC7* splicing isoforms, primers flanking the intronic sequences were used for PCR using 1 $\mu$l of cDNA diluted 1:20. PCR products were then separated on a 2% agarose gel and imaged. RT-qPCR was done in a 10-$\mu$l reaction volume with gene-specific primers using 1 $\mu$l of cDNA diluted 1:20 using Perfecta SYBR Green Fastmix (Quanta Biosciences) and a CFX96 Touch System (Bio-Rad). All samples were analyzed in triplicate for each independent experiment. RT-qPCR was also performed for the *scR1* (cytoplasmic signal recognition particle RNA subunit) RNA from each cDNA sample. Gene expression analysis was done by $2^{-\Delta Ct}$ methods using *scR1* as a reference. -Fold expression of mRNA was measured compared with WT by $2^{-\Delta\Delta Ct}$ methods (44).

### Immunoblots

Protein was isolated from cell pellets with FA-1 lysis buffer (50 mM HEPES, pH 7.5, 150 mM NaCl, 1 mM EDTA, 1% Triton X-100, 0.1% sodium deoxycholate, 1 mM PMSF, and protease inhibitors) with bead beating. The buffer was supplemented with protease inhibitor mixture tablet (Roche Applied Science). Total protein was resolved by SDS-PAGE. The gel was transferred to PVDF membrane, and proteins were detected with the following antibodies at the stated dilutions: anti-SNF2 antibody (yN-20, Santa Cruz Biotechnology) at a 1:200 dilution in 2% milk, anti-HA antibody (901514, BioLegend) at a 1:2000 dilution in 5% milk, anti-Pgk1 antibody (459250, Invitrogen) at a 1:3000 dilution in 5% milk, or anti-Coq7 antibody (described previously (16) at a 1:2000 dilution in 3% milk. Signal was detected with enhanced chemiluminescence (Thermo Scientific) as described by the manufacturer.

### Metabolic labeling of CoQ₆ with ¹³C₆-labeled precursors

Yeast strains were grown overnight in 25 ml of YPD in a shaking incubator (30 °C, 250 rpm) and diluted to an $A_{600}$ of 0.1 in 60 ml of fresh YPD the next morning. The cultures were incubated as before to an $A_{600}$ of 0.5 (midlog phase) and subsequently treated with ¹³C₆-4HB at 10 $\mu$g/ml (600 $\mu$g total) or ethanol vehicle control (0.015%, v/v). At designated time periods, cells were harvested by centrifugation at 3000 × *g* for 5 min, from 50-ml aliquots (used for lipid extraction) or 10-ml aliquots (used for RNA and protein analysis). Cell pellets were stored at −20 °C.

### Analysis of CoQ₆ and CoQ₆ intermediates

Lipid extraction of cell pellets was conducted as described (18) with methanol and petroleum ether and CoQ₄ as the internal standard. Lipid measurements were performed by HPLC-

MS/MS and normalized to total OD. Prior to mass spectrometry analysis, all samples were treated with 1.0 mg/ml benzoquinone to oxidize hydroquinones to quinones. Mass spectrometry analyses utilized a 4000 QTRAP linear MS/MS spectrometer (Applied Biosystems), and data were acquired and analyzed using Analyst version 1.4.2 and 1.5.2 software (Applied Biosystems). Separation of lipid quinones was performed with a binary HPLC delivery system and a Luna 5$\mu$ phenyl-hexyl column ($100 \times 4.6$ mm, 5 $\mu$m; Phenomenex). The mobile phase consisted of a 95:5 methanol/isopropyl alcohol solution with 2.5 mM ammonium formate as solution A and a 100% isopropyl alcohol solution with 2.5 mM ammonium formate as solution B. The percentage of solution B was increased linearly from 0 to 5% over 6 min, whereby the flow rate was increased from 600 to 800 $\mu$l. Initial flow rate and mobile phase conditions were changed back to initial phase conditions linearly over 3.5 min. Each sample was analyzed using multiple-reaction monitoring mode. The following precursor-to-product ion transitions were detected as well as the +17 *m/z* ammoniated adducts for each of the metabolic products: $^{13}C_6$-HHB *m/z* 553.4/157.0 (ammoniated: 570.4/157.0), $^{12}C$-HHB *m/z* 547.4/151.0 (ammoniated: 564.4/151.0), $^{13}C_6$-DMQ$_6$ *m/z* 567.6/173.0 (ammoniated: 584.6/173.0), $^{12}C$-DMQ$_6$ *m/z* 561.6/167.0 (ammoniated: 578.6/167.0), $^{13}C_6$-CoQ$_6$ *m/z* 597.4/203.1 (ammoniated: 614.4/203.1), $^{12}C$-CoQ$_6$ *m/z* 591.4/197.1 (ammoniated: 608.4/197.1), and $^{12}C$-CoQ$_4$ *m/z* 455.4/197.0 (ammoniated: 472.4/197.0).

### Plate dilution assays

Strains were grown overnight in 5 ml of YPD and diluted to an $A_{600}$ of 0.2 in sterile PBS. A 5-fold serial dilution in PBS was performed, after which 2 $\mu$l of each dilution ($1\times$, $5\times$, $25\times$, $125\times$, and $625\times$) were spotted onto the designated carbon sources. The final $A_{600}$ of the aforementioned dilution series are 0.2, 0.04, 0.008, 0.0016, and 0.00032, respectively.

### PHYRE homology modeling

Phyre2 is a modeling program designed to analyze protein structure, function, and mutations (45). It is used to analyze the primary sequence of a protein and, with homology detection methods, constructs a structure that compares the protein of interest with other proteins (or motifs of proteins) with known structure. In regard to Ptc7, the full nonspliced version of the protein (Ptc7$_{ns}$), which is composed of 374 amino acids and retains its 31-amino acid intron (amino acids 19–50), was analyzed. The resulting structure and alignment coverage contained 86% of residues modeled at >90% confidence, with 14% of residues modeled *ab initio*. Additionally, the spliced isoform of Ptc7 (Ptc7$_s$), which is localized and processed in the mitochondria, comprised of 305 amino acids, resulting from the removal of the 31-amino acid intron and the excision of the predicted mitochondrial targeting sequence (the 38 N-terminal amino acids of Ptc7$_s$) (46), was also modeled using the PHYRE2 intensive modeling mode. The resulting structure and alignment coverage contains 85% of residues modeled at >90% confidence, with 15% of residues modeled *ab initio*.

## References

1. Naftelberg, S., Schor, I. E., Ast, G., and Kornblihtt, A. R. (2015) Regulation of alternative splicing through coupling with transcription and chromatin structure. *Annu. Rev. Biochem.* **84,** 165–198
2. Johnson, T. L., and Vilardell, J. (2012) Regulated pre-mRNA splicing: the ghostwriter of the eukaryotic genome. *Biochim. Biophys. Acta* **1819,** 538–545
3. Pleiss, J. A., Whitworth, G. B., Bergkessel, M., and Guthrie, C. (2007) Rapid, transcript-specific changes in splicing in response to environmental stress. *Mol. Cell* **27,** 928–937
4. Ares, M., Jr., Grate, L., and Pauling, M. H. (1999) An handful of intron-containing genes produces the lion's share of yeast mRNA. *RNA* **5,** 1138–1139
5. Munding, E. M., Shiue, L., Katzman, S., Donohue, J. P., and Ares, M., Jr. (2013) Competition between pre-mRNAs for the splicing machinery drives global regulation of splicing. *Mol. Cell* **51,** 338–348
6. Venkataramanan, S., Douglass, S., Galivanche, A. R., and Johnson, T. L. (2017) The chromatin remodeling complex Swi/Snf regulates splicing of meiotic transcripts in *Saccharomyces cerevisiae*. *Nucleic Acids Res.* 10.1093/nar/gkx373
7. Hossain, M. A., Claggett, J. M., Edwards, S. R., Shi, A., Pennebaker, S. L., Cheng, M. Y., Hasty, J., and Johnson, T. L. (2016) Posttranscriptional regulation of Gcr1 expression and activity is crucial for metabolic adjustment in response to glucose availability. *Mol. Cell* **62,** 346–358
8. Hossain, M. A., Rodriguez, C. M., and Johnson, T. L. (2011) Key features of the two-intron *Saccharomyces cerevisiae* gene *SUS1* contribute to its alternative splicing. *Nucleic Acids Res.* **39,** 8612–8627
9. Jiang, L., Whiteway, M., Ramos, C. W., Rodriguez-Medina, J. R., and Shen, S.-H. (2002) The YHR076W gene encodes a type 2C protein phosphatase and represents the seventh PP2C gene in budding yeast. *FEBS Lett.* **527,** 323–325
10. Juneau, K., Nislow, C., and Davis, R. W. (2009) Alternative splicing of *PTC7* in *Saccharomyces cerevisiae* determines protein localization. *Genetics* **183,** 185–194
11. Martín-Montalvo, A., González-Mariscal, I., Pomares-Viciana, T., Padilla-López, S., Ballesteros, M., Vazquez-Fonseca, L., Gandolfo, P., Brautigan, D. L., Navas, P., and Santos-Ocaña, C. (2013) The phosphatase Ptc7 induces coenzyme Q biosynthesis by activating the hydroxylase Coq7 in yeast. *J. Biol. Chem.* **288,** 28126–28137
12. Guo, X., Niemi, N. M., Hutchins, P. D., Condon, S. G., Jochem, A., Ulbrich, A., Higbee, A. J., Russell, J. D., Senes, A., Coon, J. J., and Pagliarini, D. J. (2017) Ptc7p dephosphorylates select mitochondrial proteins to enhance metabolic function. *Cell Rep.* **18,** 307–313

13. Turunen, M., Olsson, J., and Dallner, G. (2004) Metabolism and function of coenzyme Q. *Biochim. Biophys. Acta* **1660,** 171–199

14. Doimo, M., Desbats, M. A., Cerqua, C., Cassina, M., Trevisson, E., and Salviati, L. (2014) Genetics of coenzyme Q10 deficiency. *Mol. Syndromol.* **5,** 156–162

15. Quinzii, C. M., Emmanuele, V., and Hirano, M. (2014) Clinical presentations of coenzyme Q10 deficiency syndrome. *Mol. Syndromol.* **5,** 141–146

16. Tran, U. C., and Clarke, C. F. (2007) Endogenous synthesis of coenzyme Q in eukaryotes. *Mitochondrion* **7,** S62–S71

17. González-Mariscal, I., García-Testón, E., Padilla, S., Martín-Montalvo, A., Pomares Viciana, T., Vazquez-Fonseca, L., Gandolfo Domínguez, P., and Santos-Ocaña, C. (2014) The regulation of coenzyme Q biosynthesis in eukaryotic cells: all that yeast can tell us. *Mol. Syndromol.* **5,** 107–118

18. Allan, C. M., Awad, A. M., Johnson, J. S., Shirasaki, D. I., Wang, C., Blaby-Haas, C. E., Merchant, S. S., Loo, J. A., and Clarke, C. F. (2015) Identification of Coq11, a new coenzyme Q biosynthetic protein in the CoQ-synthome in *Saccharomyces cerevisiae. J. Biol. Chem.* **290,** 7517–7534

19. Padilla, S., Jonassen, T., Jiménez-Hidalgo, M. A., Fernández-Ayala, D. J., López-Lluch, G., Marbois, B., Navas, P., Clarke, C. F., and Santos-Ocaña, C. (2004) Demethoxy-Q, an intermediate of coenzyme Q biosynthesis, fails to support respiration in Saccharomyces cerevisiae and lacks antioxidant activity. *J. Biol. Chem.* **279,** 25995–26004

20. Padilla, S., Tran, U. C., Jiménez-Hidalgo, M., López-Martín, J. M., Martín-Montalvo, A., Clarke, C. F., Navas, P., and Santos-Ocaña, C. (2009) Hydroxylation of demethoxy-Q6 constitutes a control point in yeast coenzyme Q6 biosynthesis. *Cell Mol. Life Sci.* **66,** 173–186

21. Whitehouse, I., Flaus, A., Cairns, B. R., White, M. F., Workman, J. L., and Owen-Hughes, T. (1999) Nucleosome mobilization catalysed by the yeast SWI/SNF complex. *Nature* **400,** 784–787

22. Liu, X., Li, M., Xia, X., Li, X., and Chen, Z. (2017) Mechanism of chromatin remodelling revealed by the Snf2-nucleosome structure. *Nature* **544,** 440–445

23. Dutta, A., Gogol, M., Kim, J. H., Smolle, M., Venkatesh, S., Gilmore, J., Florens, L., Washburn, M. P., and Workman, J. L. (2014) Swi/Snf dynamics on stress-responsive genes is governed by competitive bromodomain interactions. *Genes Dev.* **28,** 2314–2330

24. Dutta, A., Sardiu, M., Gogol, M., Gilmore, J., Zhang, D., Florens, L., Abmayr, S. M., Washburn, M. P., and Workman, J. L. (2017) Composition and function of mutant Swi/Snf complexes. *Cell Rep.* **18,** 2124–2134

25. Gabunilas, J., and Chanfreau, G. (2016) Splicing-mediated autoregulation modulates Rpl22p expression in *Saccharomyces cerevisiae. PLoS Genet.* **12,** e1005999

26. Neigeborn, L., and Carlson, M. (1984) Genes affecting the regulation of SUC2 gene expression by glucose repression in *Saccharomyces cerevisiae. Genetics* **108,** 845–858

27. Martín-Montalvo, A., González-Mariscal, I., Padilla, S., Ballesteros, M., Brautigan, D. L., Navas, P., and Santos-Ocaña, C. (2011) Respiratory-induced coenzyme Q biosynthesis is regulated by a phosphorylation cycle of Cat5p/Coq7p. *Biochem. J.* **440,** 107–114

28. Martin, D. E., Soulard, A., and Hall, M. N. (2004) TOR regulates ribosomal protein gene expression via PKA and the Forkhead transcription factor FHL1. *Cell* **119,** 969–979

29. Wang, A., Mouser, J., Pitt, J., Promislow, D., and Kaeberlein, M. (2016) Rapamycin enhances survival in a *Drosophila* model of mitochondrial disease. *Oncotarget* **7,** 80131–80139

30. González-Mariscal, I., Martín-Montalvo, A., Ojeda-González, C., Rodríguez-Eguren, A., Gutiérrez-Rios, P., Navas, P., and Santos-Ocaña, C. (2017) Balanced CoQ6 biosynthesis is required for lifespan and mitophagy in yeast. *Microb. Cell* **4,** 38–51

31. Sharmin, D., Sasano, Y., Sugiyama, M., and Harashima, S. (2014) Effects of deletion of different PP2C protein phosphatase genes on stress responses in *Saccharomyces cerevisiae. Yeast* **31,** 393–409

32. Marshall, A. N., Montealegre, M. C., Jiménez-Lopez, C., Lorenz, M. C., and van Hoof, A. (2013) Alternative splicing and subfunctionalization generates functional diversity in fungal proteomes. *PLoS Genet.* **9,** e1003376

33. Boukouris, A. E., Zervopoulos, S. D., and Michelakis, E. D. (2016) Metabolic enzymes moonlighting in the nucleus: metabolic regulation of gene transcription. *Trends Biochem. Sci.* **41,** 712–730

34. De, P., and Chatterjee, R. (1962) Evidence of nucleolar succinic dehydrogenase activity. *Exp. Cell Res.* **27,** 172–173

35. De, P., and Chatterjee, R. (1962) Nucleolar localization of succinic dehydrogenase in human malignant cells with MTT. *Experientia* **18,** 562

36. Yogev, O., Yogev, O., Singer, E., Shaulian, E., Goldberg, M., Fox, T. D., and Pines, O. (2010) Fumarase: a mitochondrial metabolic enzyme and a cytosolic/nuclear component of the DNA damage response. *PLoS Biol.* **8,** e1000328

37. Jung, S. J., Seo, Y., Lee, K. C., Lee, D., and Roe, J. H. (2015) Essential function of Aco2, a fusion protein of aconitase and mitochondrial ribosomal protein bL21, in mitochondrial translation in fission yeast. *FEBS Lett.* **589,** 822–828

38. Lee, S. M., Kim, J. H., Cho, E. J., and Youn, H. D. (2009) A nucleocytoplasmic malate dehydrogenase regulates p53 transcriptional activity in response to metabolic stress. *Cell Death Differ.* **16,** 738–748

39. McEwen, B. S., Allfrey, V. G., and Mirsky, A. E. (1963) Studies on energy-yielding reactions in thymus nuclei. *J. Biol. Chem.* **238,** 2571–2578

40. Monaghan, R. M., Barnes, R. G., Fisher, K., Andreou, T., Rooney, N., Poulin, G. B., and Whitmarsh, A. J. (2015) A nuclear role for the respiratory enzyme CLK-1 in regulating mitochondrial stress responses and longevity. *Nat Cell Biol.* **17,** 782–792

41. Liu, J. L., Yee, C., Wang, Y., and Hekimi, S. (2017) A single biochemical activity underlies the pleiotropy of the aging-related protein CLK-1. *Sci. Rep.* **7,** 859

42. Grate, L., and Ares, M., Jr. (2002) Searching yeast intron data at Ares lab Web site. *Methods Enzymol.* **350,** 380–392

43. Dobin, A., Davis, C. A., Schlesinger, F., Drenkow, J., Zaleski, C., Jha, S., Batut, P., Chaisson, M., and Gingeras, T. R. (2013) STAR: ultrafast universal RNA-seq aligner. *Bioinformatics* **29,** 15–21

44. Livak, K. J., and Schmittgen, T. D. (2001) Analysis of relative gene expression data using real-time quantitative PCR and the $2(-\Delta\Delta C(T))$ method. *Methods* **25,** 402–408

45. Kelley, L. A., Mezulis, S., Yates, C. M., Wass, M. N., and Sternberg, M. J. (2015) The Phyre2 web portal for protein modeling, prediction and analysis. *Nat. Protoc.* **10,** 845–858

46. Vögtle, F. N., Wortelkamp, S., Zahedi, R. P., Becker, D., Leidhold, C., Gevaert, K., Kellermann, J., Voos, W., Sickmann, A., Pfanner, N., and Meisinger, C. (2009) Global analysis of the mitochondrial N-proteome identifies a processing peptidase critical for protein stability. *Cell* **139,** 428–439

47. Ashby, M. N., Kutsunai, S. Y., Ackerman, S., Tzagoloff, A., and Edwards, P. A. (1992) COQ2 is a candidate for the structural gene encoding para-hydroxybenzoate:polyprenyltransferase. *J. Biol. Chem.* **267,** 4128–4136

48. Winzeler, E. A., Shoemaker, D. D., Astromoff, A., Liang, H., Anderson, K., Andre, B., Bangham, R., Benito, R., Boeke, J. D., Bussey, H., Chu, A. M., Connelly, C., Davis, K., Dietrich, F., Dow, S. W., *et al.* (1999) Functional characterization of the *S. cerevisiae* genome by gene deletion and parallel analysis. *Science* **285,** 901–906